

# SPHERICALLY SYMMETRIC ACCRETION FLOWS: MINIMAL MODEL WITH MHD TURBULENCE

Roman V. Shcherbakov

*Harvard-Smithsonian Center for Astrophysics, 60 Garden Street, Cambridge, MA 02138*

rshcherbakov@cfa.harvard.edu, shcher@gmail.com

## ABSTRACT

The first spherical accretion model was developed 55 years ago, but the theory is yet far from being complete. The real accretion flow was found to be time-dependent and turbulent. This paper presents the minimal MHD spherical accretion model that separately deals with turbulence. Treatment of turbulence is based on simulations of several regimes of collisional MHD. The effects of freezing-in amplification, dissipation, dynamo action, isotropization, and constant magnetic helicity are self-consistently included. The assumptions of equipartition and magnetic field isotropy are released. Correct dynamics of magnetized flow is calculated. Diffusion, convection, and radiation are not accounted for. Two different types of Radiatively Inefficient accretion flows are found: a transonic non-rotating flow (I), a flow with effective transport of angular momentum outward (II). Non-rotating flow has an accretion rate several times smaller than Bondi rate, because turbulence inhibits accretion. Flow with angular momentum transport has accretion rate about 10-100 times smaller than Bondi rate. The effects of highly helical turbulence, states of outer magnetization, and different equations of state are discussed. The flows were found to be convectively stable on average, despite gas entropy increases inward. The proposed model has a small number of free parameters and the following attractive property. Inner density in the non-rotating magnetized flow was found to be several times lower than density in a non-magnetized accretion. Still several times lower density is required to explain the observed low IR luminosity and low Faraday rotation measure of accretion onto Sgr A\*.

*Subject headings:* accretion, accretion disks — MHD — turbulence — Galaxy: center

## 1. INTRODUCTION

Dynamics of magnetized accretion flows is a major topic of astrophysical research. The problem can be solved with two different approaches: numerical and analytical. Each of them has specific difficulties, so these methods can be applied together for a better result.

Realistic numerical simulations require a lot of computational time to model even the isotropic case (Lazarian 2006). Convergence of properties of the isotropic turbulence is reached only when computational domain has more than 1024 cells in each dimension (Ladeinde & Gaitonde 2004; Biskamp 2003). Non-isotropic simulations of this size were not performed. It is also very difficult to model the system with large range of scales. The system then possesses vastly different timescales. Existing simulations of accretion flows are either axisymmetric (McKinney 2006) or consider a rather small domain close to the object (Hawley & Balbus 2002; Igumenshchev 2006). In addition, simulations should be run for sufficiently long time or several runs should be made to obtain average quantities, e.g. accretion rate, power of emitted radiation.

Analytical models do not suffer from a need to average, if they are based on averaged quantities. However, to build a reasonable model is itself difficult. No unified method exists to combine insights in physics and mathematics into a perfect analytical model. That is why the zoo of approximations of astrophysical flows is so huge.

In particular, many analytical treatments were devised for accretion: spherically symmetric treatment (Bondi 1952; Meszaros 1975; Coker & Melia 2000; Beskin & Karpov 2005), standard disk (Shakura & Sunyaev 1973), Advection-Dominated Accretion Flow (ADAF) (Narayan & Yi 1995) with its variation Hot Luminous Accretion Flow (Yuan 2001), Adiabatic Inflow-Outflow Solutions (ADIOS) (Blandford & Begelman 1999), Convection Dominated Accretion Flow (CDAF) (Narayan, Igumenshchev, & Abramowicz 2000; Quataert & Gruzinov 2000), Jet-ADAF (Yuan, Markoff, & Falcke 2002). They are aimed to describe essentially the same process: axisymmetric plasma inflow onto a compact source. Some models include the effects the others miss. Energy transport in CDAF, outflows in ADIOS are the examples. Some effects are not treated properly in any approximation.

Magnetic field is a main source of uncertainty and mistakes in theory of accretion flows. Two assumptions are usually posed to incorporate it into the model. Firstly, magnetic field is considered to be isotropic (Coker & Melia 2000; Narayan & Yi 1995). Then magnetic pressure and magnetic energy density may be put (Narayan & Yi 1995) into the dynamical equations. Secondly, the ratio of magnetic field energy density to gas thermal energy density is set to constant. This is called thermal equipartition assumption. These two ideas are at least unproven or may even not work. Magnetic field is predominantly radial in spherical

inflow (Shvartsman 1971) because of freezing-in condition and predominantly toroidal in disk (Hawley & Balbus 2002) because of magnetorotational instability.

In a good model direction and strength of the magnetic field should be determined self-consistently. Non-isotropy of magnetic field requires special dynamics. Dynamical equations were partially derived more than 20 years ago (Scharlemann 1983), but did not receive much attention or were even considered erroneous (Beskin & Karpov 2005).

Such a model may offer a natural explanation of certain accretion patterns. Accretion onto Sgr A\* gives an excellent opportunity for testing. Our Galaxy is proven to host a Supermassive Black Hole (SMBH) named Sgr A\* in its center (Ghez et al. 2003; Shen 2006). This black hole accretes matter and emits radiation with characteristic low-luminosity spectrum (Narayan et al. 1998). This spectrum was satisfactorily explained with the combination of two models: jet or non-thermal (Yuan, Quataert, & Narayan 2003) radio-emission and X-Rays with IR radiation coming from conventional ADAF flow. However, the large number of free parameters allows one to fit any spectrum well. Model with no free parameters left is an ultimate goal of the ongoing study.

Partial progress in building a self-consistent accretion model is made in this paper, which is organized as follows. Averaged spherical MHD model with turbulence is devised in Section 2. Approximate model employs the characteristic length scale about the size of the region of interest. Coefficients are taken from several hydrodynamic and MHD simulations. External sources sustain turbulence at large radii, whereas turbulence is self-sustained in the converging flow at small radii. Necessary boundary conditions are discussed in Section 3 for general flow and for Sgr A\*. Results in Section 4 are followed by the discussion of the model in Section 5. Observational implications in Section 6 are supplemented with prospects for future work and Conclusion in Section 7. Paper has several appendices.

## 2. SPHERICAL MODEL

I base all calculations on Magneto Hydrodynamic system of equations (Landau, Lifshitz & Pitaevskii 1984). The viscous terms are retained where they do not vanish in the limit of vanishing viscosity. The quantities in the following equations are fully dependent on time and coordinates. General mass flux equation reads

$$\frac{\partial \rho}{\partial t} + \nabla(\rho \mathbf{V}) = 0, \quad (1)$$

where  $\mathbf{V}$  is fluid velocity. Force balance is described by Navier-Stokes equation

$$\frac{\partial \mathbf{V}}{\partial t} + (\mathbf{V} \cdot \nabla) \mathbf{V} = -\frac{\nabla p}{\rho} - \nabla \phi_g - \frac{[\mathbf{B} \times [\nabla \times \mathbf{B}]]}{4\pi\rho} + \nu \Delta \mathbf{V}, \quad (2)$$

where  $\phi_g$  is gravitational potential,  $\nu$  is kinematic viscosity. The last term is responsible for finite energy dissipation through Kolmogorov cascade (Landau & Lifshitz 1987). Momentum equation is a combination of equations (1) and (2)

$$\frac{\partial(\rho V_i)}{\partial t} = -\frac{\partial}{\partial x_k} \left( p\delta_{ik} + \rho V_i V_k + \frac{1}{4\pi} \left( \frac{1}{2} B^2 \delta_{ik} - B_i B_k \right) \right) - \frac{\partial \phi_g}{\partial x_i} + \nu(\Delta \mathbf{V})_i. \quad (3)$$

Energy equation

$$\frac{\partial}{\partial t} \left( \frac{\rho \mathbf{V}^2}{2} + \rho \varepsilon + \frac{\mathbf{B}^2}{8\pi} \right) = -\nabla \cdot \left( \rho \mathbf{V} \left( \frac{\mathbf{V}^2}{2} + \phi_g + w \right) + \frac{1}{4\pi} [\mathbf{B} \times [\mathbf{V} \times \mathbf{B}]] + \mathbf{viscous} \right) \quad (4)$$

includes information about the equation of state. Here  $\varepsilon$  is gas internal energy density,  $w = \varepsilon + \int dp/\rho$  is gas specific enthalpy. Viscous term is responsible for diffusion. Magnetic field evolution is described by induction equation

$$\frac{\partial \mathbf{B}}{\partial t} = \nabla \times [\mathbf{V} \times \mathbf{B}] + \nu_M \Delta \mathbf{B} \quad (5)$$

with magnetic diffusivity  $\nu_M$ . Magnetic field is solenoidal as well as incompressible random velocity field:

$$\nabla \cdot \mathbf{B} = 0, \quad \nabla \cdot \mathbf{u} = 0. \quad (6)$$

## 2.1. Dynamics

Spherical accretion is the simplest pattern of all symmetric setups. We need to solve the basic model first to move then to a more realistic pattern. Construction of the minimal maximally symmetric model is the subject of the following study.

I employ the natural for the problem spherical coordinates  $(r, \theta, \phi)$  and average over angular variables  $(\theta, \phi)$ . The results depend only on the radial variable  $r$  and not on time  $t$  in the assumption that angular averaging is the same as time averaging. I need now to determine the essential quantities and derive the closed system of equations on them.

Essential quantities of a non-magnetized solution in Bondi (1952) are the inflow speed  $v(r)$ , density  $\rho(r)$ , and temperature  $T(r)$ . Turbulent magnetized case requires several more. As I release the assumption of isotropy, there are two special directions: along the radial vector  $\mathbf{e}_r$  and perpendicular to the radial vector. To describe realistic Magneto Hydrodynamic turbulence, I need at least 6 quantities: squares of radial and perpendicular magnetic fields  $B_r^2$  and  $B_\perp^2$ , squares of radial and perpendicular random fluid speeds  $u^2$  and  $u_\perp^2$ , characteristic length scale  $L$ , and dimensionless magnetic helicity  $\xi$ . The last quantity will be described

in detail in the corresponding subsection 2.4. For simplicity I consider random velocity to be isotropic and denote it as  $u(r)$ .

Total velocity of a fluid parcel

$$\mathbf{V}(r, \theta, \phi, t) = v(r)\mathbf{e}_r + \mathbf{u}(r, \theta, \phi, t) \quad (7)$$

is a sum of averaged inflow speed  $v(r)$  and instantaneous random velocity  $\mathbf{u}(r, \theta, \phi, t)$ , where by definition angular average of turbulent velocity vanishes

$$\int \mathbf{u}(r, \theta, \phi, t) d\Omega = 0. \quad (8)$$

General continuity equation (1) can be averaged with the aid of equations (6) and (8) to

$$4\pi\rho(r)v(r)r^2 = \dot{M}, \quad (9)$$

where  $\dot{M}$  is the mass accretion rate.

I derive the averaged force equation from general momentum equation (3). Tensor  $\rho V_i V_k$  averages out into the diagonal form  $\rho v^2 \delta_{rr} + \rho u^2 \delta_{ik}/3$ . Because there are no sources of magnetic field (eq. [6]) and spherical geometry is assumed, no regular magnetic field exists. Following Scharlemann (1983), I add  $B_r \nabla \mathbf{B}/(4\pi\rho)$  to the radial magnetic force  $F_r = [\mathbf{B} \times [\nabla \times \mathbf{B}]]_r/(4\pi\rho)$ , average over the solid angle, and then set  $B_\phi = B_\perp$  and  $B_\theta = B_\perp$ . Cross-terms with  $(B_\theta B_r)$ ,  $(B_\phi B_r)$ , and  $(B_\phi B_\theta)$  cancel on average over the solid angle. Finally, I obtain

$$F_r = \frac{(r^4 B_r^2)'_r}{8\pi\rho r^4} - \frac{(r^2 B_\perp^2)'_r}{4\pi\rho r^2} \quad (10)$$

for the magnetic force. I denote by  $(\cdot)'_r$  radial derivatives. I omit bulk viscosity term that results from  $\nu \Delta \mathbf{V}$ . Paczynski-Wiita gravitational potential (Paczynski & Wiita 1980)

$$\phi_g = -\frac{r_g c^2}{2(r - r_g)} \quad (11)$$

is used to imitate the effects of General Relativity, where

$$r_g = \frac{2GM}{c^2} \quad (12)$$

is a Schwarzschild radius of an object with mass  $M$ . I take gas pressure to be that of an ideal gas  $p = \rho RT/\mu$ , where  $\mu$  is a mean molecular weight. Combining all the terms, I come to the averaged force equation

$$vv'_r + \frac{r_g c^2}{2(r - r_g)^2} + \frac{R}{\mu} \frac{(\rho T)'_r}{\rho} + \frac{(\rho u^2)'_r}{3\rho} + \frac{(r^2 B_\perp^2)'_r}{4\pi\rho r^2} - \frac{(r^4 B_r^2)'_r}{8\pi\rho r^4} = 0. \quad (13)$$

Averaged energy advection equation can be derived directly from general energy equation (4). Enthalpy term should include contribution from random fluid motions as well as from gas. Isotropic random motions of fluid exert isotropic pressure  $p_{\text{rand}} = \rho u^2/3$  and have the internal energy density  $\varepsilon_{\text{rand}} = u^2/2$ . Total enthalpy  $w$  is

$$w = w_{\text{gas}} + w_{\text{rand}}, \quad \text{where} \quad w_{\text{gas}} = \frac{RT(f_e a_e(T) + f_i a_i(T) + 1)}{\mu} \quad \text{and} \quad w_{\text{rand}} = \frac{5}{6}u^2. \quad (14)$$

Fractions of electrons  $f_e \approx 0.54$  and ions  $f_i \approx 0.46$  are calculated for a gas with twice solar abundance of elements. Such high concentration of helium and metals was assumed by Baganoff et al. (2003) for spectrum fitting of Sgr A\*. Correspondent mean molecular weight is  $\mu \approx 0.7 \text{ g cm}^{-3}$ . Integral heat capacity per particle  $a_e(T)$  and  $a_i(T)$  are different for electrons and ions. Ions are non-relativistic down to  $r_g$  (Narayan & Yi 1995). Therefore  $a_i(T) = 3/2$ . General expression (Chandrasekhar 1957) should be used for thermal relativistic electrons  $a_e(T) = \Theta^{-1}(3K_3(\Theta^{-1}) + K_1(\Theta^{-1}))/ (4K_2(\Theta^{-1}) - 1)$ . Here  $\Theta = kT/m_e c^2$  is dimensionless temperature,  $K_x(Y)$  are modified Bessel functions of the second kind. Expression for non-relativistic enthalpy is

$$w_{NR} = \frac{5RT}{2\mu} + \frac{5}{6}u^2. \quad (15)$$

It is valid in the limit  $\Theta \ll 1$ . Time derivatives in energy equation (4) vanish under averaging. Equation takes the form  $\nabla \mathbf{q} = 0$ , where  $\mathbf{q}$  is the energy flux. Part of flux proportional to random velocity  $\mathbf{u}$  averages out, because turbulence is incompressible and  $u$  is zero on average (eq. [8]). Applying continuity relation (9), I finally obtain

$$vv'_r + \frac{r_g c^2}{2(r - r_g)^2} + w'_r + \frac{1}{2\pi} \left( \frac{B_{\perp}^2}{\rho} \right)'_r = 0, \quad (16)$$

where again  $B_{\theta}^2 = B_{\phi}^2 = B_{\perp}^2$ . I assumed the term  $\int [\mathbf{B} \times [\mathbf{u} \times \mathbf{B}]] d\Omega$  to also be zero along with all viscous energy transfer terms. I limit this study to Advection Dominated flows by deliberately cutting off diffusion and convection (see Appendix C).

Subtracting force equation (13) from energy advection equation (16) I get the heat balance equation that reads in non-relativistic limit

$$\frac{R}{\mu} \left( \frac{3}{2} T'_r - \frac{\rho'_r}{\rho} T \right) + \left( \left( \frac{u^2}{2} \right)'_r - \frac{\rho'_r}{\rho} \frac{u^2}{3} \right) + \frac{\rho r^2}{4\pi} \left( \frac{B_{\perp}^2}{\rho^2 r^2} \right)'_r + \frac{1}{8\pi \rho r^4} (r^4 B_r^2)'_r = 0, \quad (17)$$

similar to entropy conservation in hydrodynamics. Work done by gas is represented by  $-\rho'_r/\rho T$ . The first term has exactly the form of the second, if I make the substitution of the mean square particles velocity

$$v_p^2 = \frac{3RT}{\mu}. \quad (18)$$

Work done by the magnetic field enters the expression as derivatives of  $\rho$  and  $r$  in the magnetic part.

## 2.2. Evolution of Turbulence

Dynamics is the only part of ideal Bondi problem (Bondi 1952). In reality, flow always has some small scale turbulence that exerts back-reaction on the mean flow. The magnitude of back-reaction terms should be determined from additional equations that describe the evolution of random magnetic field and fluid motions. Since no complete theory of turbulence exists, I make a lot of approximations. The model is adjusted to agree with the results of several numerical simulations. I also apply analytical tests similar to that in Ogilvie (2003) to assure the model reproduces the basic properties of observed turbulence.

I need non-ideal induction equation (5) and Navier-Stokes equation (2) to derive how turbulence evolves. My goal is to compound reasonable equations on average squares of radial magnetic field  $B_r^2$ , perpendicular magnetic field  $B_\perp^2$ , isotropic velocity  $u^2$ . I also need equations on characteristic length scale of turbulence  $L$  and dimensionless magnetic helicity  $\xi$ .

Radial part of induction equation (5) easily gives the equation on  $B_r^2$ , when the former is multiplied by  $2B_r$  and averaged over the solid angle:

$$2B_r \frac{\partial B_r}{\partial t} = 2B_r [\nabla \times [v \mathbf{e}_r \times \mathbf{B}]]_r + 2B_r [\nabla \times [\mathbf{u} \times \mathbf{B}]]_r + 2\nu_M B_r (\Delta \mathbf{B})_r, \quad (19)$$

where indices  $()_r$  without primes denote the radial parts. The left-hand side vanishes as all time derivatives. The first term on the right-hand side represents the uniform increase of magnetic field due to flux freezing. I combine it with the continuity equation (9) to eliminate  $v$  derivatives. The second term is the dynamo action. It cannot be easily averaged. Characteristic turbulence length scale  $L$  may be used to approximate derivatives

$$\frac{\partial B_i}{\partial x_k} \sim \frac{B_i}{L} \mathbf{e}_k \quad \text{and} \quad \frac{\partial u_i}{\partial x_k} \sim \frac{u_i}{L} \mathbf{e}_k, \quad \mathbf{e}_k - \text{unit vector.} \quad (20)$$

Then we arrive at dynamo action with characteristic timescale  $\tau_{\text{dyn}} = c_{Bu} \tau_{\text{edd}}$  about eddy turn-over time  $\tau_{\text{edd}} = u/L$ . The averaged expression is quadratic in magnetic field. I take coefficient to be  $c_{Bu1}$  at any  $B_i^2$  and  $c_{Bu2}$  at any  $B_i B_k$  with  $i \neq k$ . The final form of the dynamo term reads  $2B_r [\nabla \times [\mathbf{u} \times \mathbf{B}]]_r = (c_{Bu1} B_r^2 + c_{Bu2} B_r (B_\theta + B_\phi)) u/L$ , and characteristic

$$B_r = \sqrt{B_r^2} \quad \text{and} \quad B_\theta = B_\phi = B_\perp = \sqrt{B_\perp^2} \quad (21)$$

should be taken. The last term on the right-hand side of equation (19) represents magnetic field dissipation. Dissipation term  $\nu_M \Delta \mathbf{B}$  of induction equation (5) is macroscopic in turbulence even for vanishing magnetic diffusivity  $\nu_M$  (Biskamp 2003). I approximate radial dissipation to have a timescale  $\tau_{\text{dyss}} = c_{BB} \tau_{Ar}$  about Alfvén timescale  $\tau_{Ar} = v_{Ar}/L$ . The averaged expression is also quadratic in magnetic field. I take coefficient to be  $c_{BB1}$  at any  $B_i^2$

and  $c_{BB2}$  at any  $B_i B_k$  with  $i \neq k$ . Finally,  $\nu_M B_r (\Delta \mathbf{B})_r = v_A (c_{BB1} B_r^2 + c_{BB2} (B_\theta + B_\phi) B_r) / L$ . Collecting all the terms, I obtain

$$\frac{v}{r^4} \frac{\partial (B_r^2 r^4)}{\partial r} = \frac{-(c_{Bu1} B_r^2 + 2c_{Bu2} B_r B_\perp)u + (c_{BB1} B_r^2 + 2c_{BB2} B_r B_\perp)v_{Ar}}{L} \quad (22)$$

for the radial magnetic field in the absence of external energy sources.

Perpendicular part of induction equation (5), for example  $\theta$  part, gives the equation on  $B_\theta^2$  when equation (5) is multiplied by  $B_\theta$  and averaged over the solid angle. The flux freezing condition for perpendicular field is different from that for radial field:  $B_\theta v r = \text{const}$  represents perpendicular flux freezing. I repeat the calculations made for radial field  $B_r$  to find dynamo and dissipation terms. Dynamo term takes form  $(c_{Bu1} B_\theta^2 + c_{Bu2} B_\theta (B_\phi + B_r))u / L$ . Dissipation term is  $v_{A\theta} (c_{BB1} B_\theta^2 + c_{BB2} (B_\phi + B_r) B_\theta) / L$  with perpendicular Alfvén timescale for dissipation. Here I take  $B_\perp^2 = B_\theta^2 = B_\theta B_\phi = B_\phi^2$ . Finally, I obtain

$$v \rho^2 r^2 \frac{\partial}{\partial r} \left( \frac{B_\perp^2}{\rho^2 r^2} \right) = \frac{-((c_{Bu1} + c_{Bu2}) B_\perp^2 + c_{Bu2} B_\perp B_r)u + ((c_{BB1} + c_{BB2}) B_\perp^2 + c_{BB2} B_\perp B_r)v_{A\perp}}{L}, \quad (23)$$

where continuity equation (9) is used. Radial  $v_{Ar}$  and perpendicular  $v_{A\perp}$  Alfvén speeds and random velocity  $u$  are

$$v_{Ar} = \frac{\sqrt{B_r^2}}{\sqrt{4\pi\rho}}, \quad v_{A\perp} = \frac{\sqrt{B_\perp^2}}{\sqrt{4\pi\rho}}, \quad u = \sqrt{u^2}. \quad (24)$$

Coefficients  $c_{Bu1}, c_{Bu2}, c_{BB1}, c_{BB2}$  are yet to be determined.

Evolution equation for squared random fluid velocity  $u^2$  can be found from momentum equation (3), when it is multiplied by  $2\mathbf{u}$  and averaged over the solid angle. Potential energy and pressure terms average out and only three terms are left

$$2\mathbf{u} \left( (\mathbf{V} \cdot \nabla) \mathbf{V} + \frac{\nabla(\rho \mathbf{V})}{\rho} \right) = 2 \frac{\mathbf{u} [\mathbf{B} \times [\nabla \times \mathbf{B}]]}{4\pi\rho} + 2\mathbf{u} \nu \Delta \mathbf{u}. \quad (25)$$

I apply the same averaging procedure as for magnetic field evolution equations (22) and (23). The final result is

$$v \rho^{2/3} \frac{\partial}{\partial r} \left( \frac{u^2}{\rho^{2/3}} \right) = \frac{c_{uu} u^3 - (c_{uB1} v_A^2 + (2c_{uB1} + c_{uB2}) v_{A\perp}^2 + 2c_{uB2} (v_A v_{A\perp}))u}{L}, \quad (26)$$

with additional three coefficients  $c_{uu}, c_{uB1}$  and  $c_{uB2}$ . Some of these and other  $c_{xx}$ -like coefficients can be taken from numerical simulations of isotropic turbulence, some of them can be inferred from analytical tests. They may not simply be set to convenient values like Ogilvie (2003) did.



### 2.3. Correspondence to Numerical Simulations

Isotropic turbulence is studied quite thoroughly in numerical simulations. Some results are reproduced by a number of researchers (see Biskamp (2003) for the review). That is why we may believe in these results and base a model on them. Three simulations of different turbulence regimes can provide four conditions that let us uniquely determine four combinations of coefficients  $c_{xx}$ . These regimes are decaying HD turbulence, decaying MHD turbulence, and dynamo growth of small seed magnetic field. I assume then that  $c_{xx}$  are constants independent of regime and extend the derived model to any anisotropic case.

Let me consider my model in isotropic incompressible case of box turbulence. In these settings  $B_r^2 = B_\theta^2 = B_\phi^2$ . Squared magnetic field  $B^2$  equals  $B^2 = 3B_r^2$ . Transition to the co-moving frame of averaged inflow in turbulence evolution equations (22), (23), (26) is done by stating  $d/dt = -v\partial/\partial r$ . Now I should write time derivatives instead of radius derivatives and set  $r = \text{const}$ , since matter is not moving anywhere from the box. I obtain equations of evolution of isotropic turbulent Alfven speed  $v_A$  and isotropic turbulent velocity  $u$ :

$$(u^2)'_t = \frac{\hat{c}_{uB}v_A^2u - \hat{c}_{uu}u^3}{L}, \quad (v_A^2)'_t = \frac{\hat{c}_{Bu}v_A^2u - \hat{c}_{BB}v_A^3}{L}. \quad (27)$$

Here  $v_A = \sqrt{B^2}/\sqrt{4\pi\rho}$  and  $\rho = \text{const}$ . Coefficients with hats are

$$\begin{aligned} \hat{c}_{Bu} &= c_{Bu1} + 2c_{Bu2}, & \hat{c}_{BB} &= \frac{c_{BB1} + 2c_{BB2}}{\sqrt{3}}, \\ \hat{c}_{uu} &= c_{uu1}, & \hat{c}_{uB} &= c_{uB1} + c_{uB2} \end{aligned} \quad (28)$$

in terms of previously defined  $c_{xx}$ .

I have a freedom to set  $L$ , because it enters the equations only in combinations  $c_{xx}/L$ , but  $c_{xx}$  are not yet determined. For simplicity of further derivation I take  $L(r)$  to be the effective size of energy containing eddies for isotropic incompressible turbulence:

$$u^2 = \int_{2\pi/L}^{\infty} |u_k|^2 dk \quad \text{and} \quad v_A^2 = \int_{2\pi/L}^{\infty} |v_{Ak}|^2 dk. \quad (29)$$

Isotropic decay of hydrodynamic turbulence is the simplest simulation. The convenient constant of decay is Kolmogorov constant  $C_{HD}$ . It is defined as

$$C_{HD} = E_k k^{5/3} \epsilon^{-2/3} \quad \text{with} \quad \epsilon = -\frac{d}{dt} \left( \frac{u^2}{2} \right) \quad \text{and} \quad E_k = \frac{|u_k|^2}{2}, \quad (30)$$

where  $E_k$  is energy spectrum,  $\epsilon$  is a decay rate. Kolmogorov constant was found to be  $C_{HD} \approx 1.65$  in the large set of simulations (Sreenivasan 1995). I substitute this number into equation (30) and evaluate the first integral in equation (29) to find

$$\hat{c}_{uu} = \frac{4\pi}{(3C_{HD})^{3/2}} \approx 1.14 \quad (31)$$

for isotropic equations (27).

Isotropic decay of magneto hydrodynamic turbulence gives two conditions. MHD Kolmogorov constant is defined similarly to HD case equation (30) as

$$C_{MHD} = E_k k^{5/3} \epsilon^{-2/3} \quad \text{with} \quad \epsilon = -\frac{d}{dt} \left( \frac{u^2 + v_A^2}{2} \right) \quad \text{and} \quad E_k = \frac{|u_k|^2 + |v_{Ak}|^2}{2}. \quad (32)$$

MHD turbulence is more difficult to model numerically, but the value of  $C_{MHD} \approx 2.2$  is rather rigorous (Biskamp 2003). In addition, kinetic energy was found to decay in exactly the same rate as magnetic energy. Evaluation of the sum of two integrals (29) with definitions (32) and known  $C_{MHD}$  yields

$$\hat{c}_{BB} - \hat{c}_{Bu} = \hat{c}_{uu} - \hat{c}_{uB} \approx 2\pi \left( \frac{2}{3C_{MHD}} \right)^{3/2} \approx 1.05. \quad (33)$$

Dynamo simulations explore the regime  $v_A^2 \ll u^2$ . Exponential growth of small magnetic field corresponds to some value of coefficient  $\hat{c}_{Bu}$  in equations (27) as

$$B^2 \propto \exp \left( \hat{c}_{Bu} \frac{ut}{L} \right). \quad (34)$$

External driving is purely mechanical for  $v_A^2 \ll u^2$ , so external source of magnetic field does not alter the picture of field amplification by dynamo. Characteristic length scale in dynamo simulations is usually the size of energy containing eddies  $L$  consistent with definition (29), so renormalization of length scale is not required. Older simulations (Kida, Yanase, & Mizushima 1991) have found  $b = 0.39$  that corresponds to  $\hat{c}_{Bu} \approx 0.61$ . Later results (Schekochihin et al. 2004) indicate a bit higher value  $\hat{c}_{Bu} \approx 0.7$  that I will use for my model. Finally,

$$\begin{aligned} \hat{c}_{Bu} &= 0.70, & \hat{c}_{BB} &= 1.75, \\ \hat{c}_{uu} &= 1.14, & \hat{c}_{uB} &= 0.09. \end{aligned} \quad (35)$$

The values of four  $\hat{c}_{xx}$  (eq. [35]) are not enough to obtain all seven coefficients  $c_{xx}$  in equations (22), (23), (26) with definitions (28). However, the application of common sense

analytical conditions to non-isotropic system of equations puts some additional constraints on  $c_{xx}$  that allows me to complete the model with as little guessing as possible.

Analytic tests are described in Appendix A. This completes the derivation and verification of turbulence evolution equations (22), (23), (26) with coefficients

$$\begin{aligned} c_{BB1} &= 3.03, & c_{BB2} &= 0.00, & c_{Bu1} &= 0.41, & c_{Bu2} &= 0.29, \\ c_{uu} &= 1.14, & c_{uB1} &= 0.09, & c_{uB2} &= 0.00 \end{aligned} \quad (36)$$

that I obtain summarizing equations (28), (35), (A11), and (A12). However, not all major effect have been included so far.

## 2.4. Magnetic Helicity

Certain correlation called "magnetic helicity" may strongly influence magnetic field dissipation. This quantity is defined as

$$H = \int_V (\mathbf{A} \cdot \mathbf{B}) dV, \quad (37)$$

where  $\mathbf{A}$  is a vector potential with a defined gauge condition (Biskamp 2000). Time derivative of magnetic helicity is very small compared to the time derivative of magnetic energy in high Reynolds number astrophysical plasma (Biskamp 2003):

$$\frac{dH}{dE_M} \frac{E_M}{H} \ll 1. \quad (38)$$

Constancy of magnetic helicity defines the rules of selective decay. Magnetic energy  $E_M$  decays in free turbulence down to non-zero value, allowed by constant magnetic helicity  $H = \text{const}$ . The final force-free configuration has zero random kinetic energy  $E_K$  and has aligned current density and magnetic field  $\mathbf{j} \parallel \mathbf{B}$  (Biskamp 2003).

However, the derived system of turbulence evolution equations (A1) and, therefore, equations (22), (23), (26) cannot handle selective decay. Decay of magnetic energy must be modified in order to have the transition to zero dissipation rate at certain  $v_{Ar}$  and  $v_{A\perp}$  as a function of magnetic helicity  $H$ . First, I should employ the proper magnetic helicity constancy. Then I should quantify the relation between critical  $v_{Ar}$ ,  $v_{A\perp}$ , and  $H$ .

Let me consider the region  $S$  that evolves together with the mean flow of fluid. This region has the constant angle boundaries  $\theta = \text{const}$  and  $\phi = \text{const}$ . Its radial elongation  $L_r$  scales as inflow velocity:  $L_r \propto v$ . The region  $S$  contains constant mass  $m = \text{const}$  of matter,

because matter flux through its boundaries is zero by definition. If I neglect diffusion by random velocity, frozen magnetic field lines do not move through the boundaries of the region. Because of this, magnetic helicity in  $S$  is constant  $H = \text{const}$  (Biskamp 2003).

The simplest order of magnitude relation between magnetic energy  $E_M$  and  $H$  is

$$E_M L_H = H = \text{const} \quad (39)$$

in the region  $S$ , where  $L_H$  is magnetic helicity characteristic length scale (Biskamp 2003). As magnetic field decays in turbulence,  $L_H$  grows according to equation (39).

I can parametrize  $L_H$  to be a fraction of  $L$  :

$$L_H = \xi L. \quad (40)$$

Volume of the region of interest  $S$  is

$$V = \frac{m}{\rho} \quad (41)$$

with  $m = \text{const}$ . Total magnetic energy  $E_M$  is

$$E_M = \frac{V}{8\pi} (B_r^2 + 2B_\perp^2). \quad (42)$$

I substitute relations (40), (41), and (42) into equation (39) and use the definitions (24) of Alfven velocities to come to

$$L(v_{Ar}^2 + 2v_{A\perp}^2)\xi = \text{const}. \quad (43)$$

Now I need to include  $\xi$  into the turbulence evolution equations (22), (23), (26) so that they can handle selective decay. The natural limit of  $L_H$  growth is the characteristic size of energy containing eddies  $L$ . So regime  $\xi \ll 1$  corresponds to non-helical turbulence and regime  $\xi \sim 1$  to turbulence, where magnetic helicity significantly inhibits dissipation. Regime  $\xi \gg 1$  does not occur. The basic way to modify the equations is to decrease by a smooth multiplier  $f(\xi) < 1$  magnetic field decay rate. For qualitative agreement with experiment (Biskamp 2003) I can employ

$$f(\xi) = \exp(-\xi), \quad (44)$$

what means that magnetic energy dissipation timescale becomes  $\exp(\xi)$  times larger. Terms with both  $u$  and one of  $v_{Ar}$  and  $v_{A\perp}$  in magnetic field evolution equations (22), (23) do not need to be modified, since random velocity energy decays to zero and these terms do not matter. However, I multiply the term with both random velocity and Alfven speed in turbulent velocity evolution equation (26) by  $\exp(-\xi)$  to make random velocity  $u$  decay to zero.

## 2.5. System of Equations with Source Terms

With only minor corrections, the final system of equations can be written down. In general, turbulence has external sources of energy that sustain finite magnetic and kinetic energies even in case of box turbulence. I can add source terms to incompressible system (A1) and consequently to the system of compressible equations (22), (23), (26).

System (A1) with coefficients (35) and (36), modifier (44), and source terms reads

$$\frac{d(v_{Ar}^2)}{dt} = \frac{(0.70v_{Ar}^2 + 0.58(v_{A\perp} - v_{Ar})v_{Ar})u - 3.03v_{Ar}^3 \exp(-\xi)}{L} + c_0 \frac{v_p^3}{L}, \quad (45a)$$

$$\frac{d(v_{A\perp}^2)}{dt} = \frac{(0.70v_{A\perp}^2 + 0.29(v_{Ar} - v_{A\perp})v_{A\perp})u - 3.03v_{A\perp}^3 \exp(-\xi)}{L} + c_1 \frac{v_p^3}{L}, \quad (45b)$$

$$\frac{d(u^2)}{dt} = \frac{0.09(v_{Ar}^2 + 2v_{A\perp}^2)u \exp(-\xi) - 1.14u^3}{L} + c_2 \frac{v_p^3}{L}, \quad (45c)$$

where  $v_p$  is the mean square particles speed (eq. [18]) and  $c_0$ ,  $c_1$ , and  $c_2$  are dimensionless coefficients. These coefficients determine the rates of external energy input into turbulent fields.

I denote by  $\sigma$  the ratio of total turbulent energy to thermal energy:

$$\sigma = \frac{E_K + E_M}{E_{th}}, \quad \text{so that} \quad \sigma \frac{3RT}{2\mu} = \sigma \frac{v_p^2}{2} = \frac{u^2}{2} + \frac{v_{Ar}^2}{2} + v_{A\perp}^2. \quad (46)$$

Unlike conventional plasma magnetization, magnetization  $\sigma$  with definition (46) includes the energy of random fluid motions.

In the dynamic equilibrium of constant  $v_{Ar}$ ,  $v_{A\perp}$ ,  $u$  and known  $\xi$  system (45) gives three algebraic equations for ratios  $v_{Ar}/v_p$ ,  $v_{A\perp}/v_p$ , and  $u/v_p$  as functions of  $c_0$ ,  $c_1$ , and  $c_2$ . To estimate  $c_0$ ,  $c_1$ , and  $c_2$  I take stationary driven isotropic turbulence with kinetic energy  $E_K$  equal to magnetic energy  $E_M$ . Isotropic turbulence of interest has  $v_{Ar} = v_{A\perp} = u/\sqrt{3}$ . Such turbulence occurs far from the central object, where outer magnetization is a constant  $\sigma_\infty$ . Solving system (45) I obtain using equation (46)

$$c_0 = c_1 \approx 0.124\sigma_\infty^{3/2}, \quad c_2 = 3c_0 \approx 0.371\sigma_\infty^{3/2} \quad (47)$$

in case  $\xi = 0$ . I apply these values even to turbulence with  $\xi > 0$ . Total external energy input  $Q_+$  into  $E_K$  and  $E_M$  is

$$Q_+ \approx 0.742\sigma_\infty^{3/2} \frac{v_p^3}{L}. \quad (48)$$

This energy adds up to thermal gas energy after being processed through turbulence. However, I do not adjust my dynamical equations (13) and (16) for  $Q_+$ . I self-consistently omit

external heating and radiative or diffusive cooling. This omission is physically justified sufficiently far from the central object, where cooling  $Q_-$  balances external heating  $Q_+$ . It is also justified in the inner region, where both  $Q_+$  and  $Q_-$  are negligible compared to the internal driving and energy advection. Internal driving represents build-up of self-sustained turbulence in a converging flow due to conservation of magnetic flux (Coker & Melia 2000).

Only the size  $L$  of energy containing eddies should be specified to complete the derivation of closed system of equations. In the case when energy input  $Q_+$  does not matter, the problem has only one relevant scale that is the size of the system  $r$ . Therefore, I can set  $L$  to be the fraction of radius

$$L = \gamma r \quad (49)$$

with the proportionality constant  $\gamma$  about unity. However, energy input from external sources  $Q_+$  is relatively large far from the central source. This causes medium with constant  $Q_+$ , constant  $v_p$ , and constant  $\sigma_\infty$  to have constant size of largest eddies

$$L = L_\infty = \text{const} \quad (50)$$

because of equation (48). This equality holds for radii larger than some  $r_0 \approx L_\infty/\gamma$ . I introduce a function with a smooth transition from relation (49) for  $r \ll r_0$  to relation (50) for  $r \gg r_0$ :

$$L(r) = L_\infty \left( 1 - \exp \left( -\frac{\gamma r}{L_\infty} \right) \right) \quad (51)$$

This completes derivation and verification of 8 equations (9), (13), (16), (22), (23), (26), (43), (51) with coefficients (35), (36), and (47) on 8 quantities  $L(r)$ ,  $\xi(r)$ ,  $v(r)$ ,  $u(r)$ ,  $v_{Ar}(r)$ ,  $v_{A\perp}(r)$ ,  $T(r)$ ,  $\rho(r)$  that are the characteristic turbulent length scale, normalized magnetic helicity, matter inflow velocity, turbulent velocity, radial Alfvén speed, perpendicular Alfvén speed, temperature, and density. I rewrite the equations once again in terms of named quantities:

$$4\pi\rho v r^2 = \dot{M}, \quad (52a)$$

$$v v'_r + \frac{r_g c^2}{2(r - r_g)^2} + \frac{R}{\mu} \frac{(\rho T)'_r}{\rho} + \frac{(\rho u^2)'_r}{3\rho} + \frac{(r^2 \rho v_{A\perp}^2)'_r}{\rho r^2} - \frac{(r^4 \rho v_{Ar}^2)'_r}{2\rho r^4} = 0, \quad (52b)$$

$$v v'_r + \frac{r_g c^2}{2(r - r_g)^2} + w'_r + \frac{5}{3} u u'_r + 2(v_{A\perp}^2)'_r = 0 \quad \text{with} \quad (52c)$$

$$w = w_R = \frac{RT}{\mu} \left( 0.54 \frac{3K_3(\Theta^{-1}) + K_1(\Theta^{-1})}{\Theta(4K_2(\Theta^{-1}) - 1)} + 1.69 \right) + \frac{5}{6} u^2 \quad \text{or} \quad w = w_{NR} = \frac{5RT}{2\mu} + \frac{5}{6} u^2,$$

$$v \frac{(\rho v_{Ar}^2 r^4)'_r}{\rho r^4} = \frac{3.03 v_{Ar}^3 \exp(-\xi) - (0.70 v_{Ar}^2 + 0.58(v_{A\perp} - v_{Ar})v_{Ar})u}{L} - \frac{0.64}{L_\infty} \left( \frac{RT_\infty \sigma_\infty}{\mu} \right)^{3/2}, \quad (52d)$$

$$v\rho r^2 \left( \frac{v_{A\perp}^2}{\rho r^2} \right)' = \frac{3.03v_{A\perp}^3 \exp(-\xi) - (0.70v_{A\perp}^2 + 0.29(v_{Ar} - v_{A\perp})v_{A\perp})u}{L} - \frac{0.64}{L_\infty} \left( \frac{RT_\infty \sigma_\infty}{\mu} \right)^{3/2}, \quad (52e)$$

$$v\rho^{2/3} \left( \frac{u^2}{\rho^{2/3}} \right)' = \frac{1.14u^3 - 0.09(v_{Ar}^2 + 2v_{A\perp}^2)u \exp(-\xi)}{L} - \frac{1.93}{L_\infty} \left( \frac{RT_\infty \sigma_\infty}{\mu} \right)^{3/2}, \quad (52f)$$

$$L(v_{Ar}^2 + 2v_{A\perp}^2)\xi = 3L_\infty \xi_\infty \frac{RT_\infty \sigma_\infty}{\mu}, \quad (52g)$$

$$L = L_\infty \left( 1 - \exp \left( -\frac{\gamma r}{L_\infty} \right) \right). \quad (52h)$$

Here  $\Theta = kT/m_e c^2$ . Since my prescription for external driving of turbulence is  $Q_+ = \text{const}$ , I take  $v_p$  and  $L$  to be constant in the source terms. Relativistic  $w_R$  (eq. [14]) and non-relativistic  $w_{NR}$  (eq. [15]) values of enthalpy  $w$  are employed. In the next section I describe the values of boundary conditions and parameters for the equations I solve.

### 3. BOUNDARY CONDITIONS AND PARAMETERS

The system (52) consists of 5 differential and 3 algebraic equations and should be integrated inward from some outer boundary at  $r_x$ . This requires knowledge of at least eight constants. Seven of them are the values "at infinity"  $L_\infty, T_\infty, \rho_\infty, \xi_\infty, u_\infty, v_{Ar\infty}, v_{A\perp\infty}$ . The eighth is the accretion rate  $\dot{M}$ . It is usually determined by some extra condition and is not adjustable. I assume isotropic turbulence with  $E_K = E_M$  at the outer boundary. Therefore,

$$v_{Ar\infty} = v_{A\perp\infty} = \left( \frac{RT_\infty \sigma_\infty}{\mu} \right)^{1/2} \quad \text{and} \quad u_\infty = \left( \frac{3RT_\infty \sigma_\infty}{\mu} \right)^{1/2}, \quad (53)$$

and I have one model parameter  $\sigma_\infty$  instead of 3 velocities  $v_{Ar\infty}, v_{A\perp\infty}$ , and  $u_\infty$ . Another adjustable parameter of the model is  $\gamma$  that determines the size of energy containing eddies  $L$  near the object (eq. [52h]).

Parameter  $\gamma$  is not free in principle, but its value cannot be determined within the proposed theory. Neither there exist anisotropic MHD simulations that could provide  $\gamma$ . All simulations to date show  $\gamma$  to be within  $0.2 \div 2$  (Tennekes & Lumley 1972; Landau & Lifshitz 1987; Biskamp 2003) in both HD and MHD case. I assume the same range of  $\gamma$  in my calculations.

### 3.1. Outer Medium Transition

Bondi radius

$$r_B = r_g \frac{c^2}{c_\infty^2} \quad \text{with} \quad c_\infty = \left( \frac{5RT_\infty}{3\mu} \right)^{1/2} \quad (54)$$

is the natural length scale of the spherical accretion flow (Bondi 1952). Density  $\rho$  and temperature  $T$  of plasma are constant for radii  $r \gg r_B$ , because gravitational energy and gas regular kinetic energy are negligible there compared to gas internal energy (Bondi 1952). Averaged magnetic field and averaged random velocity are also constant for  $r \gg r_B$ , because constant external energy input balances dissipation in this region. As a consequence,  $\xi = \xi_\infty$  and  $L = L_\infty$  for  $r \gg r_B$ .

I set the outer boundary at  $r_x = 3r_B$ , where matter is almost uniform. Length scale  $L_\infty$  should be determined from known external energy input  $Q_+$  and outer magnetization  $\sigma_\infty$ . However,  $Q_+$  is not known. I assume for simplicity  $L_\infty = \gamma r_B$ , so that  $L$  changes its behavior near  $r_B$  together with temperature and density.

Bondi radius is about  $r_B \approx 3 \times 10^5 r_g$  for our Galactic Center (Ghez et al. 2003). The properties of gas at  $3r_B$  are somewhat constrained from observations. I take the values for uniformly emitting gas model with temperature  $T_\infty \approx 1.5 \times 10^7$  K, electron and total number densities  $n_{e\infty} = 26 \text{cm}^{-3}$ ,  $n_\infty = 48 \text{cm}^{-3}$  (Baganoff et al. 2003) at  $r_x = 3r_B$  that corresponds to  $5''$  in the sky. The presence of dense cold component can make the average temperature much lower and the average density much higher (Cuadra et al. 2006), but I am leaving these uncertainties for future research.

Expanding and colliding hyperalfvenic stellar winds provide magnetic field into the region. Its strength near Bondi radius is not known. Only the very general estimate can be made. Matter magnetization is likely to be lower than the saturation value of  $\sigma_\infty = 1$ . I take the values in the range  $\sigma_\infty = 0.001 \div 1$  to cover all reasonable magnetization states of matter at  $3r_B$ . If magnetic field is rather a product of decay than dynamo amplification, then the local dimensionless helicity  $\xi$  may be close to unity. I cover the range  $\xi_\infty = 0.001 \div 0.5$  in simulations to determine the possible dynamical significance of non-zero magnetic helicity.

### 3.2. Transition to Rotationally Supported Flow

The system of equations (52) has the same property as spherically symmetric system of hydrodynamic equations (Bondi 1952): subsonic solution exists for all accretion rates  $\dot{M}$  up to maximum  $\dot{M}^*$ , transonic solution is valid for the only value  $\dot{M}^*$ , and no solution exists



for  $\dot{M} > \dot{M}^*$ . The solution with

$$\dot{M} = \dot{M}^* (\text{for transonic solution}) \quad (55)$$

is preferable, because it has the highest rate of energy transfer towards the equilibrium state of the system matter-SMBH. The same argument is valid for a general hydrodynamic nozzle (Landau & Lifshitz 1987). It is reasonable to expect that maximum mass flux solution for system with magnetic field (52) also obeys the condition (55). However, even small amount of angular momentum can change the picture.

Every real astrophysical accretion flow has non-zero specific angular momentum at the outer boundary

$$l = \lambda r_g c, \quad \text{or equivalently,} \quad l = v_{K\text{cir}} r_{\text{cir}}, \quad (56)$$

where  $r_{\text{cir}}$  is a radius where matter becomes rotationally supported and  $v_{K\text{cir}}$  is Keplerian velocity at  $r_{\text{cir}}$ . General Newtonian expression for Keplerian velocity at radius  $r$  is

$$v_K = c \sqrt{\frac{r_g}{2r}}. \quad (57)$$

At larger radii  $r > r_{\text{cir}}$  angular momentum exerts relatively small force  $F_l \propto l^2/r^3$  on plasma, since  $F_l$  decreases with radius faster than gravitational force  $F_g \propto r_g c/r^2$ . Numerical simulations (Cuadra et al. 2006) suggest  $r_{\text{cir}} \sim 3 \times 10^3 r_g$  for our Galactic Center.

When angular momentum (eq. [56]) is large,  $\lambda \gg 1$ , it should be able to travel outward through the outer quasi-spherical solution by means of  $r\phi$  component of stress tensor  $t_{\alpha\beta}$ . The angular averaged form of this component is

$$t_{r\phi} = \frac{\langle B_r B_\perp \rangle_\Omega}{4\pi}, \quad (58a)$$

where I neglect the kinetic part for the estimate. It can be transformed with the aid of Schwartz formula  $\langle xy \rangle \leq \sqrt{\langle x^2 \rangle} \sqrt{\langle y^2 \rangle}$  into inequality

$$t_{r\phi} \leq \frac{B_r B_\perp}{4\pi} \quad (58b)$$

with definitions (21) of rms  $B_r$  and  $B_\perp$ .

Let us take a disk (Shakura & Sunyaev 1973) with height  $H$  and write the angular momentum transfer equation as

$$\frac{d(r^2 H t_{r\phi})}{dr} = 0. \quad (59a)$$

The result of integration is (Gammie & Popham 1998)

$$\dot{M} l = 4\pi H r^2 t_{r\phi}, \quad (59b)$$

in case of large dimensionless angular momentum  $\lambda \gg 1$  (Gammie & Popham 1998). I take specific angular momentum  $l$  from equation (56) and the accretion rate to be

$$\dot{M} = 2\pi r H \rho v. \quad (60)$$

I substitute angular momentum  $l$  from relation (56), accretion rate  $\dot{M}$  from equation (60), Alfven speeds from definitions (24), Keplerian velocity from equation (57), and inequality (58b) on  $t_{r\phi}$  into angular momentum transfer equation (59b) to obtain

$$\frac{vv_K}{v_A v_{A\perp}} \sqrt{\frac{r_{\text{cir}}}{r}} = 2\chi, \quad \chi \leq 1 \quad (61a)$$

that should be valid at any radius  $r$ . Sometimes, this inequality is valid for  $r > r_{\text{cir}}$  if it is valid at  $r_{\text{cir}}$ , so that condition (61a) can in some cases be simplified to

$$\frac{vv_K}{v_A v_{A\perp}} \leq 2 \quad \text{at} \quad r_{\text{cir}}. \quad (61b)$$

Height of the disk  $H$  cancels out of final expression, thus conditions (61) are approximately valid even for flows with  $H \approx r$ . Such flows are likely to describe the realistic transition region from outer quasi-spherical inflow to inner rotational solution. There are no extra degrees of freedom to put conditions on the surface of compact object, so I consider an object to be effectively a black hole.

Condition of angular momentum transport (61) may be stronger than maximum accretion rate condition (55). This depends on the value of specific angular momentum  $l$  and viscous  $\alpha$  parameter (Shakura & Sunyaev 1973). Viscous  $\alpha$  is approximately  $\alpha \sim \chi \sigma$  according to my definitions (46) and (61a). If  $\alpha \gtrsim 0.5$ , then accretion proceeds without direct dynamical effect of rotation (Narayan, Kato, & Honma 1997). Thus, two types of solutions are possible:

- maximum accretion rate solutions that describe radial flows with small angular momentum  $l \lesssim cr_g$  or large viscosity  $\chi \sigma \gtrsim 0.5$  (subsection 4.1),
- flows with the rotational support that work for large angular momentum  $l \gg cr_g$  and small viscosity  $\chi \sigma \lesssim 0.5$  (subsection 4.2).

The condition (61) gives a crude estimate of the inflow velocity and accretion rate  $\dot{M}$ , since it assumes specific angular momentum to be constant down to  $r_{\text{cir}}$ . As matter travels to  $r_{\text{cir}}$ , the amount of specific angular momentum left becomes smaller. Nevertheless, I calculate the solutions with effective angular momentum transport using condition (61) to illustrate the dependence of accretion rate on model parameters for the rotating flow.

## 4. RESULTS

### 4.1. Maximum Rate Solution

Let me first disregard the angular momentum transport condition (61) and calculate the flow with small angular momentum  $l \ll r_g c$ , when mean rotation is not dynamically important.

The system of equations I solve (52) can be rewritten as

$$\frac{(F_i)'_r}{F_i} = \frac{N_i(\mathbf{F}, r)}{D} \quad \text{for } i = 1..8. \quad (62)$$

Here  $F_i(r)$  are 8 functions I solve for,  $N_i(\mathbf{F}, r)$  are function- and radius- dependent numerators, and

$$D = 1 - \frac{v^2}{V_s^2} \quad (63)$$

is a common denominator. Critical velocity  $V_s$  is

$$V_s^2 = c_{sg}^2 + 2v_{A\perp}^2 \quad \text{with} \quad c_{sg}^2 = c_s^2 + \frac{5u^2}{3}. \quad (64)$$

Effective sound speed  $c_{sg}$  is equal to that of plasma with effective particles velocity  $v_{pg}^2 = v_p^2 + u^2$ .

According to the maximum-rate condition (55) I search for a smooth solution that has a sonic point at some radius  $r_s$ . The condition at  $r_s$  is  $D(r_s) = 0$ . Zero denominator requires all the numerators  $N_i(\mathbf{F}, r)$  to be zero at  $r_s$ . It can be shown from system (52) that all eight conditions  $N_i(\mathbf{F}(r_s), r_s) = 0$  collapse into just one, what indicates that maximum accretion rate solution is smooth. Two equalities

$$D(r_s) = 0 \quad \text{and} \quad N_1(\mathbf{F}(r_s), r_s) = 0 \quad (65)$$

give the missing 8-th condition on  $\dot{M}$  for system (52) and the sonic radius  $r_s$ . Thus, I have 7 conditions at the boundary at  $3r_B$  and 1 condition somewhere in the region. I employ the shooting method to search for  $\dot{M}$  and  $r_s$  that satisfy the relation (65).

I obtain the Bondi hydrodynamic model (Bondi 1952), if I set all Alfven velocities and turbulent velocity to zero and use non-relativistic prescription for enthalpy  $w_{NR}$  (eq. [52c]). Therefore, the accretion rate  $\dot{M}$  equals Bondi accretion rate of monatomic gas

$$\dot{M}_B = \frac{\pi}{4} r_g^2 c^4 \rho_\infty \left( \frac{3\mu}{5RT_\infty} \right)^{3/2} \approx 4 \times 10^{-6} M_\odot \text{year}^{-1} \quad (66)$$

in the limiting case of no turbulence. The number is calculated for the Black Hole in our Galactic Center with  $r_g = 1.1 \times 10^{12} \text{cm}$  (Ghez et al. 2003),  $T = 1.5 \times 10^7 \text{K}$ , and  $n \approx 48 \text{cm}^{-3}$  (Baganoff et al. 2003). Accretion rate  $\dot{M}$  appears to be lower than  $\dot{M}_B$  when turbulent energy is non-zero (Fig. 1).

Inhibition of accretion by turbulence has the following explanation. First, energy of magnetic field increases inward, therefore it exerts back-reaction force stopping matter (Shvartsman 1971). Second, magnetic field serves a very effective mechanism of energy conversion from gravitational to thermal via dissipation of turbulence (Igumenshchev & Narayan 2002). Larger thermal energy corresponds to larger gas pressure that also stops matter. Within the deduced model I can estimate the actual decrease of accretion rate  $\dot{M}$  from Bondi value  $\dot{M}_B$ .

I take my reference model to have the values  $\gamma = 1$ ,  $\sigma_\infty = 1$ ,  $\xi_\infty = 0.025$  of, correspondingly, dimensionless scale of turbulence, outer magnetization, and outer magnetic helicity. The found accretion rates are  $0.14\dot{M}_B$  for non-relativistic equation of state and  $0.24\dot{M}_B$  for relativistic equation of state. I can now consider the whole ranges of all three parameters and explain the observed correlations between them and accretion rate  $\dot{M}$ .

Larger flow magnetization  $\sigma$  results in lower accretion rate  $\dot{M}$ . Larger magnetic field and turbulent velocity field exerts larger back-reaction force on matter. Also, transformation of gravitational energy into thermal happens more readily if magnetization is larger. Larger thermal energy means larger gas pressure and larger back-reaction force on matter striving to fall onto the central object.

Several factors lead to higher magnetization. Larger outer magnetization  $\sigma_\infty$  makes magnetization in the entire flow  $\sigma$  larger. Then larger dissipation length scale  $\gamma$  allows for smaller dissipation of magnetic field. Larger magnetic helicity  $\xi$  also lowers magnetic energy dissipation and leads to larger magnetization  $\sigma$ . These correlations can be observed on Figure 1. Increase of the relative length scale of energy containing eddies  $\gamma$  from 0.2 to 2 results (Fig. 1a) in about 2 times drop in accretion rate  $\dot{M}$ . Accretion rate stays constant (Fig. 1b) at small values of outer magnetic helicity  $\xi_\infty$ . However,  $\dot{M}$  drops an order of magnitude as turbulence approaches highly helical state at outer boundary  $3r_B$  with  $\xi_\infty$  close to 0.5. The dependence of  $\dot{M}$  on outer magnetization  $\sigma_\infty$  is not quite steep: accretion rate gradually decreases about 4 times as outer magnetization increases 3 orders of magnitude from 0.001 to 1. Surprisingly, accretion rate does not rise to  $\dot{M}_B$  (Fig. 1c) even for very small outer magnetization  $\sigma_\infty \sim 0.001$  for non-relativistic equation of state. Even small outer magnetic field increases inwards and influences flow dynamics.

Accretion rate is systematically about 40% higher (Fig. 1) for relativistic equation of

state (solid line) compared to non-relativistic equation of state (dashed line), because magnetized system has some properties of a non-magnetized one. Formula for Bondi mass accretion rate (66) is valid only for non-relativistic monatomic gas that has an adiabatic index  $\Gamma = 5/3$ . Accretion rate is higher for lower  $\Gamma$  and is about 3 times larger (Shapiro & Teukolsky 1983) in case of ultrarelativistic particles with adiabatic index  $\Gamma = 4/3$ . Accretion rate  $\dot{M}$  is determined by relation (65) at a sonic radius  $r_s$  that is smaller than  $10^3 r_g$  (Fig. 1d). Electrons become relativistic at somewhat larger radius about  $10^3 r_g$  in the solutions of system (52). This leads to gas adiabatic index  $\Gamma$  (magnetic field is disregarded) lower than  $5/3$  at sonic point  $r = r_s$ . Thus accretion rate is considerably larger in case of relativistic equation of state.

It is also instructive to trace the dependence of sonic radius  $r_s$  on parameters. Sonic radius for hydrodynamic accretion of non-relativistic monatomic gas is equal to several Schwarzschild radii  $r_s = 2 \div 10 r_g$  (Beskin & Pidoprygora 1995). Sonic radius is a considerable fraction of  $r_B$  for a gas with adiabatic index  $\Gamma$  substantially smaller than  $5/3$  for non-magnetized accretion (Bondi 1952). Magnetized accretion has the same properties. Non-relativistic EOS (solid line) results in very small sonic radius  $r_s = 7 \div 11 r_g$  (Fig. 1d). Sonic radius for relativistic EOS (dashed line) is  $r_s = 300 \div 1200 r_g$  about the radius where electrons become relativistic  $r \sim 10^3 r_g$ . The value of sonic radius drops several times as plasma outer magnetization  $\sigma_\infty$  increases from 0.001 to 1. As outer magnetization  $\sigma_\infty$  increases, accretion rate drops (Fig. 1c), because density  $\rho$  and gas inflow speed  $v$  decrease. Then effective sound speed  $V_s$  equals the inflow speed  $v$  at a point closer to the black hole.

Inflow velocity  $v$  as well as other characteristic velocities of the flow are depicted on Figure 2 as functions of radius  $r$  for the reference model with  $\sigma_\infty = 1$ ,  $\gamma = 1$ ,  $\xi_\infty = 0.025$ . All velocities are normalized to the free-fall speed

$$v_{ff} = c \sqrt{\frac{r_g}{r - r_g}}. \quad (67)$$

I also normalize perpendicular Alfvén velocity  $v_{A\perp}$  and turbulent speed  $u$  to one dimension. Horizontal line on Figure 2 corresponds to radial dependence  $r^{-1/2}$ .

Inflow velocity  $v$  monotonically increases inwards, whereas sound speed  $c_s$  monotonically decreases with intersection almost at the sonic point. Radial Alfvén velocity  $v_{Ar}$ , perpendicular Alfvén velocity  $v_{A\perp}$  and turbulent velocity  $u$  (Fig. 2) start out as constants from the outer boundary at  $3r_B$ , where turbulence is sustained by external pumping. Then these velocities increase and deviate from one another. Radial Alfvén velocity  $v_{Ar}$  appears to be much larger than  $v_{A\perp}$  and  $u$  in the inner accretion region. This fulfills the expectations of earlier models (Shakura & Sunyaev 1973; Scharlemann 1983; Beskin & Karpov 2005). At small radius turbulence is driven by freezing-in amplification of magnetic field and random

velocity. Left-hand sides of turbulence evolution equations (52d), (52e), and (52f) dominate over corresponding terms with external driving for radius  $r \lesssim 10^4 r_g$ . Internal driving of  $v_{Ar}$  is much more effective than driving of  $v_{A\perp}$  and  $u$ . Therefore radial Alfvén velocity  $v_{Ar}$  is larger than other two speeds. This refutes any model with isotropic magnetic field.

Several pairs of lines intersect on velocity plot (Fig. 2). I consider three main intersection points for the reference model with  $\sigma_\infty = 1$ ,  $\gamma = 1$ ,  $\xi_\infty = 0.025$ , and relativistic EOS (Fig. 2a). Crossing of inflow velocity  $v$  and sound speed  $c_s$  occurs almost at the sonic point at  $r_s$ , determined by relation (65) with critical velocity  $V_s$  (eq. [64]). No plasma waves can escape from within the region with high inflow velocity  $v > V_s$ . Approximately  $c_s \approx V_s$  at sonic point  $r_s \approx 6 \times 10^{-4} r_B$ , because of low magnetization  $\sigma \approx 20\%$  in that region (Fig. 3a). Alfvén point is determined by equality  $v = v_{Ar}$  at radius  $r_A$ . Alfvén waves cannot escape from within the region where inflow speed is greater than radial Alfvén speed  $v_{Ar}$ . Equality holds at relatively large radius  $r_A \approx 0.03 r_B$ . The third combination of the same three velocities also gives a characteristic intersection point. Radial Alfvén speed  $v_{Ar}$  increases faster inwards and becomes equal to sound speed  $c_s$  at about  $r \approx 4 r_g$ . Further relative increase of  $v_{Ar}$  leads to magnetic energy dominated flow, what can be traced on magnetization plot (Fig. 3a).

Figure 3a shows evolution of plasma magnetization  $\sigma$  with radius  $r$  for the reference model. Thermal energy equipartition assumption does not hold, id est turbulent energy does not equal to constant fraction of thermal energy  $\sigma \neq \text{const}$ . Magnetization  $\sigma$  varies more than one order in magnitude from 0.07 to 3. It starts out at initial  $\sigma_\infty = 1$  at  $3 r_B$ , where turbulence is supported by external energy input  $Q_+ = \text{const}$ . Then  $\sigma$  deviates down as  $r$  decreases. Magnetization  $\sigma$  drops, because length scale  $L$  decreases with radius  $r$  that causes turbulence to decay faster. At about  $0.03 r_B$  magnetization starts to rise as internal turbulence driving takes over. Inflow velocity  $v$  slightly deviates up from Alfvén velocity  $v_A$  as  $r$  decreases. Since internal driving rate is proportional to  $v$  (left-hand sides of equations (52d), (52e), and (52f) dissipation rate is proportional  $v_{Ar}$ , parameter  $\sigma$  grows slightly with decreasing radius. The growth is about a factor of 5 for 3.5 orders of magnitude decrease in radius. Magnetization  $\sigma$  jumps up in the region very close to the event horizon of the black hole. However, this jump may originate from inconsistent treatment of General Relativity.

The dependence of magnetic helicity  $\xi$  on radius is shown on Figure 3b. Helicity  $\xi$  behaves almost reciprocally to magnetization  $\sigma$  from Figure 3a. Such a behavior can be seen from magnetic helicity equation (52g). Magnetization  $\sigma$  decreases order of magnitude during the transition from externally supported to internally supported turbulence around  $r \approx 0.03 r_B$ . Magnetic helicity  $\xi$  also increases an order of magnitude from 0.025 to 0.2. Then  $\xi$  gradually decreases down to initial value. Thus magnetic helicity  $\xi$  does not change dynamics if it is initially small  $\xi_\infty \lesssim 0.1$ . Only when  $\xi_\infty$  is large, accretion rate drops.

Deviation of inflow velocity  $v$  from the free-fall scaling  $r^{-1/2}$  makes a density profile in magnetized flow different from that in standard Advection Dominated Accretion Flow (ADAF). I consider the flow where energy is only advected inward. Nevertheless, I obtain

$$\rho \propto r^{-\zeta} \quad \text{with} \quad \zeta \approx 1.25 \quad (68)$$

almost independently on the parameters or the equation of state, somewhat shallower than  $\rho \propto r^{-1.5}$  in ADAF.

The only question left is how well this flow with maximum accretion rate can describe the real situation with large angular momentum  $l$ . Given the solution of the system (52) I can check whether the condition for effective angular momentum transport condition (61) holds. Condition (61) breaks when evaluated for maximum-rate solution with parameters  $\xi_\infty$ ,  $\sigma_\infty$ , and  $\gamma$  within the chosen ranges and circularization radius  $r_{\text{cir}} > r_g$ . This means a flow with maximum accretion rate is unable to effectively transport the angular momentum outward. The same conclusion can be made simpler. The transport of angular momentum is a magnetic process. So,  $l$  can be transported only by Alfven waves. However, Alfven waves cannot escape from the region within  $r_A \approx 0.03r_B$  from the compact object that makes angular momentum transport impossible even from quite large radius.

## 4.2. Solution with Effective Angular Momentum Transport

Solution with large outer angular momentum  $l \gg r_g c$  and small viscosity may have properties, substantially different from those of maximum-rate solution. The actual details of the solution and allowed accretion rate depend on how this angular momentum is transported. For the simple estimate I suppose that the accretion rate is determined by the equality in angular momentum transport condition (61). Maximum accretion rate  $\dot{M}$  for condition (61) appears to be about two orders of magnitude lower than Bondi rate  $\dot{M}_B$  (eq. [66]).

I add one parameter in modelling: unknown circularization radius  $r_{\text{cir}}$  for specific angular momentum  $l$  (eq. [56]). I take it to be  $r_{\text{cir}} = 10^3 r_g$  for the reference model. Plots of the accretion rate verses model parameters are shown on Figure 4. Dependencies for the rotating solution (Fig. 4) have the opposite slopes to those for the maximum-rate solution on Figure 1. Accretion rate  $\dot{M}$  increases with increasing outer magnetization  $\sigma_\infty$  (Fig. 4b) and increasing outer magnetic helicity  $\xi_\infty$  (Fig. 4c). Both effects lead to higher plasma magnetization  $\sigma$ . I showed in the previous subsection 4.1 that the magnetic field plays an inhibiting role on matter inflow, and that the larger the magnetic field is, the smaller the accretion rate  $\dot{M}$  is. However, the correlation between the magnetic field and accretion rate is the opposite in case of the rotating flow. Accretion rate quantitatively agrees with relation for ADAF flows

$\dot{M} \sim \alpha \dot{M}_B \sim \sigma \chi \dot{M}_B$  (Narayan, Kato, & Honma 1997) with  $\sigma \sim 0.01$  at  $r_{\text{cir}}$  (Fig. 6a).

The allowed by condition (61) inflow speed  $v$  is proportional to the product of radial Alfvén speed  $v_{Ar}$  and perpendicular Alfvén speed  $v_{A\perp}$ . Larger magnetic field results in larger transport of angular momentum outward, so larger inflow velocity  $v$  and larger accretion rate are possible. Larger outer magnetization  $\sigma_\infty$  and larger outer magnetic helicity  $\xi_\infty$  both lead to higher magnetization  $\sigma$  and higher magnetic field. Inhibiting effect of magnetic field is smaller in case of lower accretion rates  $\dot{M}$  and lower inflow velocities  $v$ . Lower  $v$  results in lower relative driving of turbulence that makes magnetic field weaker. Weaker magnetic field has weaker influence on dynamics. In sum, larger magnetic field  $B$  results in larger accretion rate  $\dot{M}$ , when it needs to transfer angular momentum.

The dependence of  $\dot{M}$  on length scale  $\gamma$  is obscured by the dependence of external driving on  $\gamma$ . Accretion rate  $\dot{M}$  is smaller for smaller magnetic field, but the state of low magnetization can be achieved in two different ways. Firstly, magnetic field decays faster when  $L$  decreases. However, the plasma at circularization radius  $r_{\text{cir}} = 10^3 r_g$  is still partially influenced by the outer boundary conditions. Internal driving does not depend on  $L$ , whereas external driving is stronger and magnetization  $\sigma$  is higher, when  $L$  is small. The described two effects balance each other and make accretion rate  $\dot{M}$  almost independent of dimensionless length scale  $\gamma$  (Fig. 4a).

Accretion rate  $\dot{M}$  decreases with the decrease of circularization radius  $r_{\text{cir}}$  (Fig. 4d) for non-relativistic equation of state. To explain this, I trace on Figure 5b all the quantities that enter angular momentum transport condition (61b) for the reference model. Velocities normalized by the free-fall speed (eq. [67]) are shown on Figure 5b. Inflow speed  $v$  and radial Alfvén velocity  $v_{Ar}$  reach free-fall scaling at about  $0.02 r_B$ . Only perpendicular Alfvén velocity  $v_{A\perp}$  has a different dependence on distance from the central object for  $r < 0.02 r_B$ . Because  $v_{A\perp}$  decreases with radius, the allowed  $v$  and  $\dot{M}$  are smaller for smaller circularization radius.

However, the accretion rate increases for small circularization radii for 1-T equation of state (Fig. 4d, solid line). This is the consequence of the decreasing gas adiabatic index, when electrons reach relativistic temperatures. Solutions with lower adiabatic index are known to have larger accretion rates (Bondi 1952) that is equivalent to the lower inflow speeds  $v$  in the solutions for the fixed matter inflow rate. Velocity  $v$  (Fig. 5a) starts deviating down from the self-similar  $r^{-1/2}$  solution at approximately  $10^3 r_g$ , making the solutions with higher  $\dot{M}$  possible. In fact, condition (61) for the solutions with small  $r_{\text{cir}}$  becomes critical at some fixed point  $r_d > r_{\text{cir}}$  instead of reaching equality at  $r_{\text{cir}}$  (eq. [61b]). Therefore, according to condition (61a), maximum value of the inflow speed grows with the decrease of circularization radius as  $v \propto r_{\text{cir}}^{-1/2}$ , explaining the rise of accretion rate for small  $r_{\text{cir}}$  (Fig. 4d, solid line) for 1-T equation of state.



Solution for non-relativistic equation of state, in turn, possess its own feature. Self-similar flow (see Appendix B) settles in at  $10^3 r_g$ , making accretion rate almost independent on circularization radius (Fig. 4d). Magnetic helicity  $\xi$  in such a flow is a number about unity what is consistent with self-similar solution obtained in Appendix B. Self-similar flow can not establish for 1-T equation of state, because relativistic effects become important before it establishes and break self-similarity.

In fact, magnetization  $\sigma$  and magnetic helicity  $\xi$  (Fig. 6) are not constant at small radii for correct 1-T EOS, because these relativistic corrections work. At about  $0.01 r_B$  magnetization reaches almost constant level  $\sigma \approx 0.02$  (Fig. 6a) and then starts to slightly deviate down, because equilibrium  $\sigma$  for matter with lower gas adiabatic index  $\Gamma < 5/3$  is lower. Magnetic helicity  $\xi$  behaves (Fig. 6b) the opposite way to magnetization  $\sigma$  : magnetic helicity reaches  $\xi \approx 1.5$  at  $0.01 r_B$  and starts to slightly deviate up as the radius decreases.

## 5. DISCUSSION OF THE MODEL

I present the sophisticated analytical model to determine the properties of spherical magnetized accretion. The common assumptions of magnetic field isotropy and thermal equipartition are released, but many assumptions are still left. As usually in fluid dynamics a lot of simplifications are made during the course of elaboration. The validity of almost everything can be questioned. The system of equations (52) may not describe the real flow (subsection 5.1) or may have some inaccuracies (subsection 5.2). Gas cooling may not be neglected (subsections 5.3). Convection and diffusion may change the flow structure (subsection 5.4). The equation of state was also found to influence the dynamics (subsection 5.5). Let me discuss all these topics and determine the practical significance of the model.

### 5.1. Real Flow

Presented model is partially applicable to the real systems. It may describe some gas flows onto Supermassive Black Holes in Low Luminosity Galactic Centers, in particular in the center of our Galaxy. These flows are geometrically thick (Narayan & Yi 1995) and may have low angular momentum (Moscibrodzka, Das, & Czerny 2006). However, the real flows may have properties that my model cannot handle in its current state. First of all, the sources of matter and external driving should be explicitly accounted for. Secondly, the self-consistent angular momentum transport theory is needed.

The material is mainly supplied to the central parsec of the Milky Way by stellar winds

(Quataert 2004). The wind-producing stars have a broken power-law distribution as a function of radius (Baganoff et al. 2003). Some stars are as close to the central black hole as  $0.1r_B$  (Ghez et al. 2003). The stars supply too much material to be accreted, therefore there exist an outflow (Quataert 2004). Bondi radius coincides with the radius where inflow starts to dominate outflow in numerical simulations with the accretion rate  $\dot{M} \sim 10^{-6} M_\odot \text{year}^{-1}$  (Cuadra et al. 2006). Maximum accretion rate in the solution with zero angular momentum is  $0.2\dot{M}_B \approx 10^{-6} M_\odot \text{year}^{-1}$  and  $0.01\dot{M}_B$  for the rotating flow. So that the transition from the outflow to the inflow happens at  $r \gtrsim 10^5 r_g$ .

I can show that outflow from  $r \gtrsim 10^5 r_g$  does not change the accretion rate from calculated. Outflows substantially alter the value and the sign of inflow velocity  $v$  in the system (52). However, the differences in inflow velocity do not influence any other quantity as long as three conditions are satisfied:

1.  $v$  is much smaller than gas particles velocity  $v_p$ , bulk kinetic energy of gas is negligible in the outflow region,
2. external driving of turbulence  $Q_+$  dominates over internal driving there,
3. condition on  $\dot{M}$  is set in the inflow region.

The first two conditions are satisfied down to  $r \sim 10^4 r_g$  (Fig. 2 and Fig. 5). The third condition holds for maximum rate solution, because condition on  $\dot{M}$  is set at the sonic point about  $10^3 r_g$  from the central object. It also hold for the solution with angular momentum transport, because the condition on  $\dot{M}$  is usually set at the inner boundary  $10^3 \div 10^4 r_g$ . All three above conditions hold, hence outflows of stellar winds do not substantially change the accretion rate or any quantity in the system.

## 5.2. Treatment of Magnetic Field

The long history of accretion theory has many accepted models based on ideas, extended beyond the area of applicability of these ideas. For example, general relativity was substituted with Paczynski-Wiita gravitational potential (Paczynski & Wiita 1980; Shakura & Sunyaev 1973). Magnetic field was long treated similar to the normal matter (Narayan & Yi 1995; Coker & Melia 2000). Displacement current was neglected in magnetic field dynamics that allowed to treat magnetic field without electric field (Scharlemann 1983). System of viscous equations describe viscosity by a single parameter (Shakura & Sunyaev 1973; Landau & Lifshitz 1987; Landau, Lifshitz & Pitaevskii 1984; Biskamp 2003). Gyrokinetics is used to solve the problems with non-Maxwellian distribution functions (Sharma et al.

2007), power-law non-thermal electrons are usually present in plasma (Yuan, Markoff, & Falcke 2002).

Described above model is extended in several ways, mainly with regard to magnetic field. Isotropic MHD system of turbulent equations (27) describes the real box collisional turbulence quite well, because it corresponds to convergent set of simulations. Collisionality assumes that medium behaves like many particles with short-range interactions. However, astrophysical medium of interest is always collisionless with prevailing long-range interactions. I inconsistently use the results of numerical simulations of collisional MHD (eqs. [1-6]) with magnetic resistivity  $\nu_M$  on the order of viscosity  $\nu$ , because the realistic simulations of collisionless plasma turbulence are not done and are unlikely to be done in the near future (Schekochihin et al. 2004).

Observations of astrophysical turbulence may give more information than numerical simulations. A special case of collisionless plasma is plasma with random kinetic energy much smaller than random magnetic energy. This regime is a good picture of Sun corona with all plasma effects into play (Aschwanden 2005). Dissipation of magnetic loops with low kinetic energy proceeds mainly via reconnections. The timescale of reconnective dissipation was found to be

$$\tau_{\text{rec}} \approx 20 \frac{L}{v_A} \quad (69)$$

in solar flares (Noglik, Walsh, & Ireland 2005). The same number was also predicted by Lazarian & Vishniac (1999). Collisional MHD turbulence has much smaller dissipation timescale

$$\tau_{\text{diss}} \approx 1 \frac{L}{v_A} \quad (70)$$

(eqs. [27, 35]). Plasma has large kinetic energy in the outer region of accretion flow, where turbulence is externally supported. Timescale  $\tau_{\text{diss}}$  (eq. [70]) may be appropriate there. Kinetic energy  $E_K$  decreases to smaller radii and magnetization  $\sigma$  increases (Fig. 2) in case of zero angular momentum (4.1). Accretion flow there may resembles solar Corona (Aschwanden 2005). Dissipation timescale may increase order of magnitude and be close to  $\tau_{\text{rec}}$  (eq. [69]). This increase would lead to much lower accretion rate, because higher magnetic field leads to lower  $\dot{M}$ . Matter infall may eventually proceed through channels of lower magnetic field (Igumenshchev 2006).

Even if I assume that box isotropic turbulent system of equations (27) with coefficients (35) is applicable to isotropic turbulence, there are at least four complications in building the full anisotropic theory.

First of all, I need to introduce arbitrary coefficients  $c_{uB2}$ ,  $c_{BB2}$ ,  $c_{Bu2}$  to describe isotropization of anisotropic magnetic field and anisotropic energy transfer between mag-

netic field and fluid motions. Reasonable values of these coefficients were taken to satisfy rather loose analytical tests (Appendix A). However, changes in these coefficients do not lead to dramatically different accretion rate or flow structure. Setting  $c_{BB2} = c_{BB1}$  instead of  $c_{BB2} = 0$  leads to only 10% of  $\dot{M}$  change for the reference model. All seven introduced coefficients  $c_{xx}$  may themselves depend on anisotropy of the magnetic field. The details of anisotropic MHD are still debatable (Goldreich & Sridhar 1995; Boldyrev 2006). I leave the incorporation of anisotropic MHD model into accretion theory for future work.

Secondly, the presented theory is not general relativistic. Accretion rate  $\dot{M}$  appears to be insensitive to the choice of gravitational potential. The condition on  $\dot{M}$  is set at about  $10^3 r_g$  in case of relativistic EOS and zero angular momentum  $l$ . Sonic point is situated close to the black hole at  $r_s = 5 \div 10 r_g$  for non-relativistic equation of state. But 1% increase of  $\dot{M}$  leads to the sonic point at  $r_s > 100 r_g$ , independent of the way to mimic general relativity. However, the region near the black hole is important, because part of synchrotron IR radiation as well as part of radio emission comes from several Schwarzschild radii (Narayan et al. 1998; Falcke & Markoff 2000; Marrone 2007). Thus, to fully constrain theory by observations general relativistic magnetohydrodynamics is a must.

In third, magnetic helicity  $H$  involves numerous complications. Magnetic helicity evolves in the region that is frozen into matter. The distance  $L_{||}$  between radial boundaries of this region is proportional to inflow velocity  $v$ , thus  $L_{||}$  increases with increasing  $v$  and at some point  $L_{||} > r$ , whereas size in the angular direction is about  $L = \gamma r$ . A part of the region is getting sucked into the black hole, while a part is still situated at fairly large radius  $r$ . Equation of magnetic helicity evolution (52g) holds only if I assume even redistribution of magnetic helicity over the mass of plasma. This holds for frozen magnetic field, but in reality diffusion and convection are present. Diffusion may change the results for  $H$  (eq. [52g]) as well as for the entire flow pattern. I also leave these uncertainties for future research.

In fourth, it was recently suggested by Beskin & Karpov (2005) that ions and electrons should be viewed in accretion as confined by magnetic field lines. This is the opposite of standard picture where magnetic field lines are frozen into matter (Scharlemann 1983). The former case has higher heating rate of matter under contraction (Beskin & Karpov 2005), because of conservation of the first adiabatic invariant  $I = 3cp_t^2/(2eB) = \text{const}$  (Landau & Lifshitz 1975). Here  $p_t$  is a particles momentum in the direction perpendicular to  $\mathbf{B}$ . However, only highly magnetized flows with magnetization  $\sigma > 1$  conserve  $I$ . Non-linear collective interactions of particles in low- $\sigma$  plasma are likely to isotropize their distribution. When particles are heated isotropically under contraction, general Magneto-Hydrodynamics (eqs. [1-6]) works (Landau, Lifshitz & Pitaevskii 1984) and heating rate stays unchanged. Magnetization in computed models is below unity (Fig. 3a and Fig. 6a). Thus application

of first adiabatic invariant conservation to magnetized accretion flow seems irrelevant.

Finally, mean rotation of the flow also creates anisotropy. Because the inner gas rotates faster than the outer, MagnetoRotational Instability (MRI) works. It produces the additional driving of magnetic field that may be concurrent to other sources. MRI (Hawley & Balbus 2002) has a timescale

$$\tau_{MRI} = - \left( r \frac{d(l/r^2)}{dr} \right)^{-1}. \quad (71)$$

When MRI timescale becomes larger than dynamic timescale  $\tau_{dyn} = r/v$ , field amplification occurs mainly because of regular shear tangential motion, instead of regular radial motion. MRI may be crucial even in the region without rotational support. Full consideration of effects of angular momentum on the flow is the subject of the next study.

### 5.3. Radiative Cooling

The system of equations (52) describes the accretion flow, where all the energy is stored in the same piece of matter where it initially was. There is no energy loss by diffusive or radiative cooling. But whether such a model is realistic.

Let me estimate the radiative cooling first. Line cooling is more effective than bremsstrahlung cooling for temperatures about  $T_\infty \approx 1.5 \times 10^7 K$ . Line cooling function is  $\Lambda \approx 6 \times 10^{-23} n^2 (T/10^7 K)^{-0.7}$  erg cm<sup>-3</sup> s<sup>-1</sup> (Sutherland & Dopita 1993). Thus characteristic cooling time  $\tau_{cool}$  is

$$\tau_{cool} = \frac{3RT\rho}{2\Lambda\mu} \approx 1 \times 10^{12} \text{s} \quad (72)$$

for our Galactic Center accretion. The dynamic timescale  $\tau_{dyn} = r/v$  for accretion with rate  $\dot{M} = 0.1\dot{M}_B$  (eq. [66]) is

$$\tau_{dyn} = \frac{\rho r^3}{\dot{M}} \approx 5 \times 10^{10} \text{s} \quad (73)$$

with continuity equation (9) at radius  $r = r_B$  (eq. [54]). Cooling time is about 20 times larger than inflow time in the region where outflows dominate. Nevertheless, anisotropy of stellar winds may lead to significant cooling of some clumps of matter (Cuadra et al. 2005). Even the disk may form (Cuadra et al. 2006). Careful calculation with line cooling is yet to be done.

## 5.4. Convection & Diffusion

The system (52) does not include diffusive or convective transport of quantities. Thus the system represents Advection-Dominated flow, where magnetic field and gas can exchange energy between each other. The exact model would include transport of momentum, energy, magnetic field, magnetic helicity that may or may not influence the dynamics.

First of all, any type of convective or diffusive motion would happen at a speed  $v_c$  not exceeding the maximum of turbulent speeds, radial Alfvén speed  $v_c < v_{Ar}$ . This leads to the transition from convection dominated to advection dominated flow at several dozens  $r_g$  in the case with rotation (Abramowicz et al. 2002). Correspondingly, inflow speed  $v$  becomes large  $v_c \sim v$  (Gammie & Popham 1998). Transport becomes ineffective at  $r \lesssim r_A$ , where  $r_A$  is the radius of Alfvén point. According to Fig. 2a, Alfvén point in my spherical solutions lies at  $r_A \sim 0.03r_B$ . Thus diffusion and convection are strongly suppressed in the inner flow. By the same reason, magneto-thermal instability (MTI) (Parrish & Stone 2005) is not supposed to play any role for spherical inflow, but may play a role in a case with rotation. For the non-conductive convective stability criterion see Appendix C.

However, speed of electrons  $v_e$  may overcome the speed of sound  $c_s$ , so electron conduction may in principle transport energy from within  $r_A$  (Johnson & Quataert 2007). It is yet unclear whether electron conduction is suppressed at high inflow velocity  $v > v_{Ar}$ , because electrons may be bound to the field lines of tangled magnetic field. The efficiency of conduction is a free parameter. If efficiency is close to maximum and conduction is not inhibited, then accretion rate may be 1 ÷ 2 orders of magnitude lower than Bondi rate  $\dot{M}_B$  (Johnson & Quataert 2007), thus accretion rate would be limited by conduction and not by backreaction of the magnetic field. Other types of energy transport (Parrish & Stone 2005) may kick in for lower accretion rates. The correct calculation with magnetic field and better prescription for conductivity is yet to be done.

## 5.5. Equation of State

The difference in accretion rate  $\dot{M}$  between one-temperature relativistic and 1-T non-relativistic EOSs is up to 40% for maximum-rate solution (subsection 4.1) and up to several times for solution with effective angular momentum transport (subsection 4.2). Solution with smaller gas adiabatic index  $\Gamma$  has larger accretion rate  $\dot{M}$  (Shapiro & Teukolsky 1983). Gas adiabatic index gradually falls from  $\Gamma = 5/3$  to  $\Gamma = 1.43$  in case of relativistic EOS as matter approaches the black hole.

However, the electron temperature  $T_e$  is unlikely to be equal to ion temperature  $T_i$ .

Electron temperature  $T_e$  is usually modelled to be lower than  $T_i$  (Narayan & Yi 1995). This two-temperature model has lower gas pressure support and larger gas adiabatic index  $\Gamma$  than 1-T model with  $T = T_i$ . Lower gas pressure leads to higher accretion rate, larger  $\Gamma$  leads to lower accretion rate. The combination of these two effects is expected to change the accretion rate by about the same 40% as between relativistic and non-relativistic 1-T EOSs. The exact details depend on the two-temperature model chosen.

## 6. OBSERVATIONS

Proposed quasi-spherical magnetized accretion model is aimed to explain plasma flow onto SuperMassive Black Hole Sgr A\* in our Galactic Center. Many observations of this source are made. These observations reasonably agree with the results of my model.

A common misconception about Chandra X-Ray observations of Sgr A\* exists in literature. X-Rays mainly originate in the region that lies further than Bondi radius  $r_B$  from the central object. Thus characteristic density  $\rho_\infty$  and temperature  $T_\infty$  far from the Black Hole can be found (Baganoff et al. 2003). If one knows the mass  $M$ , this automatically gives Bondi accretion rate  $\dot{M}_B$  (eq. [66]). However, accretion rate is not necessarily determined by this formula (66), unlike some papers suggest (Bower et al. 2005). In my model accretion rate  $\dot{M}$  is independent on radius and is smaller than  $\dot{M}_B$ .

IR (Eckart et al. 2006) and Radio (Shen 2006) observations are difficult to interpret, because fluxes in these diapasons depend strongly on the accretion model. Density of matter  $\rho$  is better constrained by observations than accretion rate  $\dot{M}$ . The general agreement (Yuan, Markoff, & Falcke 2002) is that density  $\rho$  should be lower than in Bondi solution  $\rho_B$  in the region close to the black hole. Solutions with outflows (Yuan, Quataert, & Narayan 2003) and Convectively-Dominated flows (Quataert & Gruzinov 2000) were invented to explain this lower density. Magnetized solution without angular momentum does well the same job. Let me consider the reference magnetized model with  $\sigma_\infty = 1$ ,  $\gamma = 1$ ,  $\xi_\infty = 0.025$ ,  $l = 0$ , 1-T relativistic equation of state. The ratio of density in a reference magnetized model to density in a non-magnetized solution is

$$\frac{\rho_{\text{magn}}}{\rho_{\text{nonmagn}}} \approx 0.27 \quad \text{at} \quad 10r_g. \quad (74)$$

Density in a magnetized model is much lower than in a non-magnetized one. However, all types of models can be made to fit the data by adjusting temperature (Quataert & Gruzinov 2000), whether advection dominated or convection or outflow dominated.

Faraday rotation of submillimeter radiation offers a good differentiation mechanism be-

tween ADAF flows and flows with outflows or convection. Rotation measure is proportional to both magnetic field and electron density and has a relativistic temperature factor (Marrone 2007). Model *B* predicts magnetization  $\sigma = 0.7$  and number density  $n = 2 \cdot 10^7 \text{cm}^{-3}$  at  $3r_g$  that is consistent with (Hawley & Balbus 2002). The observed Faraday rotation measure is  $\text{RM} = -6 \cdot 10^{-5} \text{rad m}^{-1}$ . (Marrone 2007). Fitting the relativistic rotation measure for temperature gives  $T_e = 4 \cdot 10^{10} \text{ K}$  in excellent agreement with (Sharma et al. 2007). Accretion rate in the reference model is about  $9 \cdot 10^{-7} M_\odot \text{year}^{-1}$ , what is 30 times lower than in (Sharma et al. 2007). However, the electron density in my model is close to that in the rotating model (Sharma et al. 2007), because inflow velocity in the rotating model is  $\alpha$  times lower. For densities to agree I need  $\alpha \sim 0.03$  that is somewhat smaller than found in numerical simulations  $\alpha \gtrsim 0.2$  (Hawley & Balbus 2002). This means my solution overestimates density  $n$  by about a factor of 5, what results in larger then observed IR flux (Eckart et al. 2006). Effects of angular momentum transport, outflows (Yuan, Markoff, & Falcke 2002) or conduction (Johnson & Quataert 2007) must come into play to allow for successful fitting for both IR flux and Faraday rotation measure.

## 7. CONCLUSIONS

Though many ways of dealing with inefficient accretion were invented, my approach is substantially different from all previous efforts. **I elaborated the model that**

- has very few free parameters,
- self-consistently includes averaged turbulence, combining geometrical effects of freezing-in amplification with dissipation,
- ties evolution of random magnetic field and random velocity field to numerical simulations,
- connects outer externally supported turbulence to inner self-sustained turbulence,
- predicts the accretion rates  $\dot{M}$  and flow patterns for the flows with negligible angular momentum,
- gives the order of magnitude estimate of  $\dot{M}$  for large angular momentum flows.

**The model predicts**

- accretion rate  $\dot{M}$  of magnetized fluid  $0.2 \div 0.7$  of Bondi rate  $\dot{M}_B$  even for small outer magnetization  $\sigma_\infty$ ,



- subequipartition magnetic field in the outer part of the flow and superequipartition in the inner part,
- several times lower density than in Bondi model near the central object, what with addition of other effects would explain the observations of Sgr A\*,
- half an order of magnitude effect of different equations of state on the accretion rate,
- unimportance of magnetic helicity conservation,
- ineffectiveness of convection. Convection and diffusion should be accounted for together.

**The next version of the model will include**

- more anisotropic effects, in particular, magneto-rotational instability,
- two-temperature equations of state,
- full treatment of angular momentum transport,
- diffusion of momentum, heat and magnetic field.

## 8. ACKNOWLEDGEMENTS

The author is grateful to Ramesh Narayan for fruitful discussions. The author thanks Pascal Demoulin for useful comments about magnetic helicity and Ya. N. Istomin for general comments.

## REFERENCES

- Abramowicz, M. A., Igumenshchev, I. V., Quataert, E., & Narayan, R. 2002, ApJ, 565, 1101
- Aschwanden, M. J. 2005, Physics of the Solar Corona: An Introduction with Problems and Solutions, (2d ed.; Chichester, UK: Springer)
- Baganoff, F. K., et al. 2003, ApJ, 591, 891
- Beskin, G. M., & Karpov S. V. 2005, A&A 440, 223
- Beskin, V. S., Pidoprygora, Yu. N. 1999, JETP, 80, 575

- Biskamp, D. 2000, "Magnetic reconnection in plasmas", (Cambridge, UK: Cambridge University Press)
- Biskamp, D. 2003, "Magnetohydrodynamic turbulence", (Cambridge, UK: Cambridge University Press)
- Bisnovatyi-Kogan, G. S., & Ruzmaikin, A. A. 1974, *Ap&SS*, 28, 45
- Blandford, R. D., & Begelman, M. C. 1999, *MNRAS*, 303L, 1
- Boldyrev S. 2006, *Phys. Rev. Lett.*, 96, 5002
- Bondi, H. 1952, *MNRAS*, 112, 195
- Bower, G. C., Falcke, H., Wright, M. C., Backer, & Donald C. 2005, *ApJ*, 618, 29
- Chandrasekhar, S. 1957, "Introduction to the Study of Stellar Structure", (New York: Dover Publications)
- Coker, R.F., Melia, F. 2000, *ApJ*, 534, 723
- Cuadra, J., Nayakshin, S., Springel, V., & Di Matteo, T. 2005, *MNRAS*, 360L, 55
- Cuadra, J., Nayakshin, S., Springel, V., & Di Matteo, T. 2006, *MNRAS*, 366, 358
- Eckart A., et. al. 2006, *A&A*, 450, 535
- Falcke, H., & Markoff, S. 2000, *A&A*, 362, 113
- Gammie, C. F., & Popham, R. 1998, *ApJ*, 498, 313
- Ghez, A. M., Becklin, E., Duchjne, G., Hornstein, S., Morris, M., Salim, S., & Tanner, A. 2003, *ANS*, 324, 527
- Goldreich, P., Sridhar, S. 1995, *ApJ*, 438, 763
- Hawley, J. F., & Balbus, S. A. 2002, *ApJ*, 573, 738
- Igumenshchev, I. V., & Narayan, R. 2002, *ApJ*, 566, 137
- Igumenshchev, I. V. 2006, *ApJ*, 649, 361
- Johnson, B. M., Quataert, E. 2007, *ApJ*, 660, 1273
- Kida, S., Yanase, S., & Mizushima, J. 1991, *Phys. Fluids A*, 3, 457

- Ladeinde, F., & Gaitonde, D. V. 2004, *Phys. Fluids*, 16, 2097
- Landau, L. D., & Lifshitz, E. M. 1975, "Classical theory of fields", (Oxford: Pergamon Press)
- Landau, L. D., & Lifshitz, E. M. 1987, "Fluid mechanics", (Oxford: Pergamon Press)
- Landau L. D., Lifshitz E. M., & Pitaevskii L. P. 1984, "Electrodynamics of Continuous Media", (Oxford: Pergamon Press)
- Lazarian, A., & Vishniac, E. T. 1999, *ApJ*, 517, 700
- Lazarian, A., 2006, *Int. J. Mod. Phys. D*, 15, 1099
- Marrone, D. P., Moran, J. M., Zhao, J., & Rao R., 2007, *ApJ*, 654L, 57
- McKinney J. C. 2006, *MNRAS*, 368, 1561
- Meszaros P. 1975, *Nature*, 258, 583
- Moscibrodzka, M., Das, T. K., & Czerny, B. 2006, *MNRAS*, 370, 219
- Narayan, R., & Yi, I. 1995, *ApJ*, 452, 710
- Narayan, R., Kato, S., Honma, F. 1997, *ApJ*, 476, 49
- Narayan, R., Mahadevan, R., Grindlay, J. E., Popham, R. G., & Gammie, C. 1998, *ApJ*, 492, 554
- Narayan, R., Igumenshchev, I. V., & Abramowicz, M. A. 2000, *ApJ*, 539, 798
- Narayan, R., Quataert, E., Igumenshchev, I. V., & Abramowicz, M. A. 2002, *ApJ*, 577, 295
- Noglik, J. B., Walsh, R. W., & Ireland, J. 2005, *A&A*, 441, 353
- Ogilvie, G. I. 2003, *MNRAS*, 340, 969
- Paczynski, B., & Wiita, P.J. 1980, *A&A*, 88, 23
- Parrish, I. J., Stone, J. M. 2005, *ApJ*, 633, 334
- Quataert, E., & Gruzinov, A. 2000, *ApJ*, 539, 809
- Quataert, E., & Gruzinov, A. 2000, *ApJ*, 545, 842
- Quataert, E. 2004, *ApJ*, 613, 322
- Scharlemann, E.T. 1983, *ApJ*, 272, 279

- Schekochihin, A. A., Cowley, S. C., Taylor, S. F., Maron, J. L., & McWilliams, J. C. 2004, *ApJ*, 612, 276
- Shakura, N. I., & Syunyaev, R. A., 1973, *A&A*, 24, 337
- Sharma, P., Quataert, E., Hammett, G. W., & Stone, J. M. 2007, *ApJ*, 667, 714
- Shapiro S. L., & Teukolsky S. A. 1983, "Black holes, white dwarfs, and neutron stars: The physics of compact objects", (New York: Wiley-Interscience)
- Shvartsman, V.F. 1971, *Soviet Astronomy*, 15, 377
- Sreenivasan, K. R. 1995, *Phys. Fluids*, 7, 2778
- Sutherland, R. S., & Dopita, M. A. 1993, *ApJS*, 88, 253
- Tennekes H., & Lumley J. L. 1972, "A First Course in Turbulence", (Cambridge: MIT Press)
- Yuan, F. 2001, *MNRAS*, 324, 119
- Yuan, F., Markoff, S., & Falcke, H. 2003, *ANS*, 324, 453
- Yuan, F., Quataert, E., & Narayan, R. 2003, *ApJ*, 598, 301
- Yuan, F., Taam, R. E., Xue, Y., & Cui, W. 2006, *ApJ*, 636, 46
- Shen, Zhi-Qiang 2006, *J. Phys. Conf. Ser.*, 54, 377

## A. ANALYTICAL TESTS

Let me consider my model in anisotropic incompressible case of box turbulence. I substitute  $-v\partial/\partial r = d/dt$  in equations (22), (23), (26) and set  $r = \text{const}$ . The box has infinite volume. I express some of unknown  $c_{xx}$  in terms of known  $\hat{c}_{xx}$  from equations (28). The system now reads

$$\frac{d(v_{Ar}^2)}{dt} = \frac{(\hat{c}_{Bu}v_{Ar}^2 + 2c_{Bu2}(v_{A\perp} - v_{Ar})v_{Ar})u - (\sqrt{3}\hat{c}_{BB}v_{Ar} + 2c_{BB2}(v_{A\perp} - v_{Ar}))v_{Ar}^2}{L}, \quad (\text{A1a})$$

$$\frac{d(v_{A\perp}^2)}{dt} = \frac{(\hat{c}_{Bu}v_{A\perp}^2 + c_{Bu2}(v_{Ar} - v_{A\perp})v_{A\perp})u - (\sqrt{3}\hat{c}_{BB}v_{A\perp} + c_{BB2}(v_{Ar} - v_{A\perp}))v_{A\perp}^2}{L}, \quad (\text{A1b})$$

$$\frac{d(u^2)}{dt} = \frac{(\hat{c}_{uB}(v_{Ar}^2 + 2v_{A\perp}^2) - c_{uB2}(v_{Ar} - v_{A\perp})^2)u - c_{uu}u^3}{L}. \quad (\text{A1c})$$

I need to determine three coefficients  $c_{BB2}$ ,  $c_{uB2}$ , and  $c_{Bu2}$  and prove the entire system (A1) makes sense.

There are three kinds of analytical tests divided by the degree of their certainty. The tests from the first group have solid physical grounds. The tests from the second group represent how turbulence is believed to work, these are the general relations with clear physical insight. The third group of tests consists of the order of magnitude relations and the disputable ideas.

The tests of the first group are proven to work. Only one test of this kind can be applied to our system. This is the energy decay test. Free incompressible MHD turbulence has decreasing with time total energy, because energy decrease corresponds to the increase of entropy of the system gas/magnetic field (Landau, Lifshitz & Pitaevskii 1984).

$$\frac{d}{dt} \left( \frac{v_{Ar}^2 + 2v_{A\perp}^2 + u^2}{2} \right) < 0 \quad \text{for at least one of } v_{Ar}, v_{A\perp}, u \text{ non-zero.} \quad (\text{A2})$$

I take sum with proper coefficients of the right-hand sides of system (A1). Then I maximize it with respect to  $v_{A\perp}/v_{Ar}$  and  $v_A/u$ . I find that when

$$2c_{Bu2} + c_{uB2} \geq -2.2, \quad (\text{A3})$$

total energy decreases with time for any non-zero  $v_{Ar}$ ,  $v_{A\perp}$ , and  $u$ . Let me remind the reader that all these velocity are non-negative according to definitions (24). Condition (A3) is weak. Some tests from the second and the third categories constrain  $c_{uB2}$  and  $c_{Bu2}$  better, thus making equation (A3) valid.

The typical test of the second category deals with dynamo amplification of anisotropic field. Dynamo action not only amplifies magnetic field, but also isotropizes it. I take isotropization condition to be

$$\frac{d(v_{Ar} - v_{A\perp})}{dt(v_{Ar} - v_{A\perp})} \leq 0. \quad (\text{A4})$$

Taking expressions for derivatives from system (A1) I arrive at

$$(\hat{c}_{Bu} - 3c_{Bu2})u - \sqrt{3}c_{BB2}(v_{Ar} + v_{A\perp}) + c_{BB2}(2v_{Ar} + v_{A\perp}) \leq 0 \quad (\text{A5a})$$

This condition should hold when any speed in inequality (A5a) is much larger then two others. Therefore, inequality (A5a) is equivalent to

$$\hat{c}_{Bu} < 3c_{Bu2}, \quad c_{BB2} < \frac{\sqrt{3}}{2}\hat{c}_{BB}. \quad (\text{A5b})$$

Another second category dynamo test states that magnetic field should always increase, if dynamo operates without dissipation or any energy transfer. This occurs when Alfvén speeds are much smaller than turbulent velocity field  $u$ . Positive amplification condition then reads

$$\frac{dv_{Ar}^2}{dt v_{Ar}^2} > 0, \quad \frac{dv_{A\perp}^2}{dt v_{A\perp}^2} > 0. \quad (\text{A6})$$

Taking the expressions for derivatives from system (A1) and applying the limit  $v_{Ar} \ll u$  and  $v_{A\perp} \ll u$  I obtain that inequalities (A6) are valid for any balance between  $v_{Ar}$  and  $v_{A\perp}$  when

$$\hat{c}_{Bu} > 2c_{Bu2}. \quad (\text{A7})$$

Inequalities (A5b) and (A7) give tight constraints on  $c_{Bu2}$ .

The similar test exists for the random velocity. Magnetic field is supposed to increase the turbulent velocity in the limit  $v_{Ar} \sim v_{A\perp} \gg u$ . The correspondent condition

$$\frac{d}{dt} \left( \frac{u^2}{2} \right) > 0 \quad \text{for} \quad v_{Ar} \sim v_{A\perp} \gg u \quad (\text{A8})$$

reduces for system (A1) to the condition of constant positive acceleration that initially steady magnetic field applies to matter. Finally

$$c_{uB2} < \hat{c}_{uB}. \quad (\text{A9})$$

Decay of isotropic MHD turbulence offers the following test of the second kind. Numerical simulations show equality of magnetic field dissipation rate and random velocity dissipation rate (33) when initial magnetic energy equals initial kinetic energy. However, this equality should be stable, otherwise kinetic and magnetic energy would diverge from each other after any perturbation and equality of  $u$  and  $v_A$  would not have been observed. Stability condition is

$$\frac{d(v_{Ar}^2 + 2v_{A\perp}^2 - u^2)}{dt (v_{Ar}^2 + 2v_{A\perp}^2 - u^2)} < 0 \quad (\text{A10})$$

for  $v_{Ar} = v_{A\perp} = u$ .

There are no more proven or justified assumptions I can make. I need to make use of inequalities (A3), (A5b), (A7), (A9), and (A10) and apply unjustified tests. I take the value of  $c_{Bu2}$  to be in the middle of the allowed interval

$$c_{Bu2} = \frac{1}{2} \left( \frac{1}{2} + \frac{1}{3} \right) \hat{c}_{Bu} \approx 0.29. \quad (\text{A11})$$

The value of  $c_{uB}$  is small compared to the values of other coefficients. There is no physical sense in the sharp increase of  $u^2$  build-up when magnetic field becomes anisotropic that would be the case for  $c_{uB2} \ll (-\hat{c}_{uB})$ . Turbulent velocity may be expected to increase regardless of the direction of magnetic field in equation (A1c). This idea leads to  $|c_{uB2}| < \hat{c}_{uB}$ . I take

$$c_{uB2} = 0 \tag{A12}$$

for the simple estimate. Similar estimate allows me to set

$$c_{BB2} = 0. \tag{A13}$$

In this case isotropization of magnetic field has a timescale about the dissipation timescale.

## B. SELF-SIMILAR SOLUTION

Let me describe the self-similar solution, when the differential system of equations (52) can be reduced to the algebraic system. I set the proper scalings of quantities with radius and make weak additional assumptions. I introduce the standard dimensionless variables  $T(x), \rho(x), L(x), aa(x), bb(x), pp(x), vel(x)$  to replace, respectively,  $T(r), \rho(r), L(r), u(r), v_{Ar}(r), v_{A\perp}(r), v(r)$  as follows:

$$\begin{aligned} T(r) &= T_\infty T(x), & v(r) &= vel(x) \left( \frac{2RT(x)}{\mu} \right)^{1/2}, & L(r) &= (r/x)L(x), \\ u(r) &= aa(x) \left( \frac{2RT(x)}{\mu} \right)^{1/2}, & v_{Ar}(r) &= bb(x) \left( \frac{2RT(x)}{\mu} \right)^{1/2}, & v_{A\perp}(r) &= pp(x) \left( \frac{2RT(x)}{\mu} \right)^{1/2}. \end{aligned} \tag{B1}$$

Radius is normalized to Bondi radius (eq. [54]) as  $r = r_B x$ . The natural power-law radial dependencies of these quantities (B1)

$$\begin{aligned} T(x) &= T_{SS} x^{-1}, & vel(x) &= v_{SS} x^{-1/2}, & L(x) &= \gamma, \\ aa(x) &= u_{SS} x^{-1/2}, & bb(x) &= v_{ArSS} x^{-1/2}, & pp(x) &= v_{A\perp SS} x^{-1/2} \end{aligned} \tag{B2}$$

make my system of equations (52) independent of  $x$  under the following restrictions:

- gravity is Newtonian,
- external turbulence driving is negligible,

- equation of state is non-relativistic.

These assumptions are valid in the intermediate region  $10^3 r_g \lesssim r \lesssim 0.1 r_B$ . Gravity is Newtonian for  $r \gg r_g$ . Turbulence driving is mainly internal for  $r \lesssim 0.1 r_B$  (see subsections (4.1), (4.2) and Fig. 1b, Fig. 5b). Electrons become relativistic at around  $10^3 r_g$ . The found range of  $r$  where all above assumptions hold is small. I can instead consider a non-relativistic equation of state with  $w = w_{NR}$  (eq. [52c]) everywhere. This makes standard self-similar solution possible from  $0.1 r_B$  down to several Schwarzschild radii  $r_g$ .

Dimensionless magnetic helicity  $\xi$  appears to be constant in self-similar regime. Relations (52h), (52g), and (46) lead to

$$\xi = \frac{3\sigma_\infty}{4T_{SS}(v_{ArSS}^2 + 2v_{A\perp SS}^2)}\xi_\infty. \quad (\text{B3})$$

Continuity equation (52a) can be used to obtain the scaling of density  $\rho \sim x^{-3/2}$ . Heat balance equation (17) reduces to the equality of radial and total perpendicular magnetic fields

$$v_{ASS}^2 = 2v_{A\perp SS}^2. \quad (\text{B4})$$

Euler equation (52b) gives the formula for self-similar temperature

$$T_{SS} = 5/(15 + 10u_{SS}^2 + 9v_{ArSS}^2 + 6v_{A\perp SS}^2 + 6v_{SS}^2). \quad (\text{B5})$$

Turbulence evolution equations (22), (23), (26) are now treated without source terms. They give, correspondingly, three relations

$$\begin{aligned} 2u_{SS}v_{ArSS}c_{Bu11} - 2v_{ArSS}^2c_{BB11}\exp(-\xi) + 4u_{SS}c_{Bu22}v_{A\perp SS} + 3v_{ArSS}v_{SS}\gamma &= 0, \\ 2u_{SS}(v_{ArSS}c_{Bu22} + (c_{Bu11} + c_{Bu22})v_{A\perp SS}) - v_{A\perp SS}(2c_{BB11}\exp(-\xi)v_{A\perp SS} + 3v_{SS}\gamma) &= 0, \quad (\text{B6}) \\ -u_{SS}^2c_{uu} + c_{uB11}\exp(-\xi)(v_{ArSS}^2 + 2v_{A\perp SS}^2) &= 0, \end{aligned}$$

where definitions of Alfven and turbulent velocities (24) are used.

Let me first set magnetic helicity to zero  $\xi = 0$  and consider four equations (B4) and (B6) on four velocities  $v_{SS}$ ,  $u_{SS}$ ,  $v_{ArSS}$ ,  $v_{A\perp SS}$ . The only solution of this system has all the velocities identical zeroes. No self-similar solution is possible for zero magnetic helicity  $\xi$ .

However, the non-linear algebraic system of equations on  $\xi$  and velocities (B3), (B4), (B6) possesses a non-trivial self-similar solution. For the full system (52) I need the additional condition to determine the accretion rate and solve for radial dependencies of quantities. This condition is either condition for maximum accretion rate (64) or condition for effective



angular momentum transport (61). I can transform both into self-similar form. Maximum  $\dot{M}$  condition (64) reads

$$5 + 10u_{SS}^2 + 12v_{A\perp SS} = 6v_{SS}^2. \quad (\text{B7a})$$

Effective angular momentum transport condition (61) gives

$$\frac{\sqrt{5/3} v_{SS}}{4v_{ArSS} v_{A\perp SS} \sqrt{T_{SS}}} \leq 1 \quad (\text{B7b})$$

regardless of circularization radius  $r_{\text{cir}}$ .

Let me first find the self-similar solution in case of large angular momentum. I solve equality in relation (B7b) and 5 equations (B3), (B4), (B5), (B6) for 7 quantities  $\xi$ ,  $T_{SS}$ ,  $u_{SS}$ ,  $v_{ArSS}$ ,  $v_{A\perp SS}$ ,  $\gamma v_{SS}$ , and the product  $\sigma_\infty \xi_\infty$ . I normalize the results to free-fall velocity (eq. [67]) to be able to directly compare with the numbers on Figure 5b:

$$\frac{c_s(r)}{v_{ff}(r)} = 0.58, \quad \frac{u(r)}{\sqrt{3}v_{ff}(r)} = 0.0094, \quad \frac{v_{Ar}(r)}{v_{ff}(r)} = 0.041, \quad (\text{B8})$$

$$\frac{v_{A\perp}(r)}{v_{ff}(r)} = 0.029, \quad \frac{v(r)}{v_{ff}(r)} = 0.0033, \quad \sigma_\infty \xi_\infty = 0.00718 \quad (\text{B9})$$

for  $r \gg r_g$ . Figure 5b shows profiles of velocities for the reference model with  $\sigma_\infty = 1$ ,  $\xi_\infty = 0.025$ ,  $\gamma = 1$ . The actual velocities on the inner boundary at  $r = 3 \times 10^{-4} r_B = 90r_g$  are

$$\begin{aligned} \frac{c_s(r)}{v_{ff}(r)} &= 0.58, & \frac{u(r)}{\sqrt{3}v_{ff}(r)} &= 0.0033, & \frac{v_{Ar}(r)}{v_{ff}(r)} &= 0.076, \\ \frac{v_{A\perp}(r)}{v_{ff}(r)} &= 0.024, & \frac{v(r)}{v_{ff}(r)} &= 0.0051. \end{aligned} \quad (\text{B10})$$

The reference model has  $\sigma_\infty \xi_\infty = 0.025$  about 3 times larger than in self-similar solution (B8), magnetic field in the reference model is stronger. Therefore, higher values of all characteristic velocities are expected in the actual solution (B10). I obtain inflow velocity  $v$  and radial Alfven speed  $v_{Ar}$  correspondingly 1.5 and 1.8 times higher for solution (B10). Sonic speeds are the same in self-similar (B8) and actual (B10) solutions, because almost all gravitational energy goes into thermal energy in both cases. However, perpendicular Alfven velocity  $v_{A\perp}$  and turbulent velocity  $u$  do not qualitatively agree with self-similar solution. They are correspondingly 1.2 and 2.8 times lower in the actual solution (B10). The naive estimate for accretion rate is

$$4\pi\rho_\infty v(r_B) r_B^2 \approx 0.05 \dot{M}_B. \quad (\text{B11})$$

This appears to be 8 times larger than the actual accretion rate  $0.0061 \dot{M}_B$ . Velocity near Bondi radius (eq. [54]) is much smaller than self-similar value, what leads to an overestimate

of  $\dot{M}$ . Thus, self-similar solution can give an order of magnitude estimates for all characteristic velocities of the flow and even for accretion rate  $\dot{M}$ . However, self-similar solution has only 2 free parameters instead of 3, because  $\sigma_\infty \xi_\infty$  is treated as one constant. Therefore, solution of the full system (52) is required to probe the entire parameter space and to achieve more precise results.

Self-similar solution in case of maximum rate flow with condition (B7a) does not exist. The formal solution of equations (B7a), (B3), (B4), (B6) leads to negative product  $\sigma_\infty \xi_\infty$ . The absence of self-similar solution in this case is reasonable, since the actual solution does not exhibit self-similar scalings (Fig. 1b).

### C. CONVECTION

Let me elaborate the stability criterion against convection in my model. As I noted in the main text (subsection 5.4), small scale perturbations of quantities are smeared out by diffusion. Thus high-frequency analysis by Scharlemann (1983) is not appropriate to determine the convective stability. Timescale of diffusion  $\tau_{\text{diff}}$  is

$$\tau_{\text{diff}} \sim \frac{h}{u}, \quad (\text{C1})$$

where  $l$  is the scale of perturbation. As  $h$  decreases, diffusion time also decreases and becomes smaller than perturbation growth timescale  $\tau_{\text{grow}}$ . If  $\tau_{\text{diff}} < \tau_{\text{grow}}$ , convection is ineffective that is likely to happen at small scales  $h$ . Thus I need to consider the motion of the large blobs of the size  $h \sim L$ .

I consider a blob of plasma displaced at some small  $\Delta r$  from its equilibrium position (Fig. 7). The density of the blob itself changes by  $\Delta \rho_{\text{blob}}$ , when it is moved. The density of outer medium changes by  $\Delta \rho_{\text{fluid}}$  between two positions of the blob. The goal is to calculate the difference in density differences  $\Delta \rho_{\text{fluid}} - \Delta \rho_{\text{blob}}$  between the outer medium and the blob. Positive difference  $\Delta \rho_{\text{fluid}} - \Delta \rho_{\text{blob}} > 0$  for positive  $\Delta r > 0$  implies convective instability. Rising blob of gas is rarified compared to the fluid and buoyant. The results for  $\Delta \rho$  may be affected by external driving that is somewhat artificial in my model. Thus I need to calculate  $\Delta \rho$  in the inner accretion region where external driving is not important. Motion of the blob is adiabatic and governed by the same adiabatic dynamical equations (52b) and (52c), as the rest of the fluid. I neglect energy, associated with gas regular velocity  $v$ . Term  $v^2$  cannot be neglected only in the region, where  $v$  approaches sound speed  $c_s$ . However, convection ceases if  $v \sim c_s$  (Narayan et. al. 2002). I denote by index  $A$  physical quantities in the blob and by index  $F$  quantities in the rest of the fluid.

Euler equation (52b) results in the following equations on differences in the blob

$$\frac{R}{\mu}\Delta_A(\rho T) + \frac{1}{3}\Delta_A(\rho u^2) + \frac{1}{r^2}\Delta_A(r^2\rho v_{A\perp}^2) - \frac{1}{2r^4}\Delta_A(r^4\rho v_A^2) = 0 \quad (\text{C2a})$$

and in the fluid

$$\frac{R}{\mu}\Delta_F(\rho T) + \frac{1}{3}\Delta_F(\rho u^2) + \frac{1}{r^2}\Delta_F(r^2\rho v_{A\perp}^2) - \frac{1}{2r^4}\Delta_F(r^4\rho v_A^2) = 0. \quad (\text{C2b})$$

In both equations I take variations between quantities at  $r + \Delta r$  and  $r$ . I introduce the difference operator

$$\Delta() = \Delta_F() - \Delta_A() \quad (\text{C3})$$

and calculate the variations of all quantities between the fluid and the blob. Subtracting equation (C2b) from equation (C2a), I find the radial pressure balance in the first order in  $\Delta r$

$$\frac{R}{\mu}\Delta(\rho T) + \frac{1}{3}\Delta(\rho u^2) + \Delta(\rho v_{A\perp}^2) - \frac{1}{2}\Delta(\rho v_A^2) = 0. \quad (\text{C4})$$

Blob of plasma should be in equilibrium also in perpendicular direction, not only in radial direction. I use the same technique to deduce it, as I used to derive the radial force equation (13) from general momentum equation (3). Component  $\theta$  of magnetic force in equations (2) and (3) reads  $F_\theta = [\mathbf{B} \times [\nabla \times \mathbf{B}]]_\theta / (4\pi\rho)$ . I subtract  $B_\theta(\nabla \times \mathbf{B}) / (4\pi\rho)$  from it and average over  $\phi$  direction. I obtain

$$F_\theta = \frac{(B_r^2)'_\theta}{8\pi\rho r} \quad (\text{C5})$$

for  $B_\theta^2 = B_\phi^2$  and  $B_r B_\theta = 0$  on average over  $\phi$ . The final form of force balance in  $\theta$  direction is

$$\frac{\partial}{\partial\theta} \left( \frac{R}{\mu}\rho T + \frac{1}{3}\rho u^2 + \frac{1}{2}\rho v_A^2 \right) = 0. \quad (\text{C6})$$

Perpendicular force balance (C6) has the same form in any direction perpendicular to the radial vector owing to the symmetry of the problem. I apply operator  $\Delta$  (eq. [C3]) to the integral form of perpendicular pressure balance and get

$$\frac{R}{\mu}\Delta(\rho T) + \frac{1}{3}\Delta(\rho u^2) + \frac{1}{2}\Delta(\rho v_A^2) = 0. \quad (\text{C7})$$

Heat balance equation (17) gives the third relation

$$\frac{R}{\mu} \left( \frac{3}{2}\Delta T - \frac{\Delta\rho}{\rho}T \right) + \left( u\Delta u - \frac{u^2}{3}\frac{\Delta\rho}{\rho} \right) + \rho\Delta \left( \frac{v_{A\perp}^2}{\rho} \right) + \frac{1}{2\rho}\Delta(\rho v_A^2) = 0. \quad (\text{C8})$$

Expansion or contraction of a blob is non-uniform. Perpendicular  $b$  and parallel  $a$  sizes (Fig. 7) deform in different ways. Continuity equation for the fluid (9) can be written as

$$\frac{\Delta_F \rho}{\rho} + \frac{\Delta_F v}{v} + 2 \frac{\Delta r}{r} = 0 \quad (\text{C9a})$$

I consider the parcel with constant mass  $m = \rho V$ . Therefore

$$\frac{\Delta_A \rho}{\rho} + \frac{\Delta a}{a} + 2 \frac{\Delta b}{b} = 0 \quad (\text{C9b})$$

is the continuity relation for the parcel. Finally I subtract equation (C9a) from equation C9b and obtain

$$\frac{\Delta \rho}{\rho} + \frac{\Delta v}{v} + 2 \frac{\Delta r}{r} - \frac{\Delta a}{a} - 2 \frac{\Delta b}{b} = 0 \quad (\text{C10})$$

for the change of density according to definition (C3). Inflow velocity  $v$  is clearly associated with the fluid, but I omit subscript  $F$  at  $v$ . I also omit subscript  $A$  at dimensions of the blob.

Now I need to quantify the variation of the turbulent magnetic field and the random velocity. I assume that the blob moves at a speed  $V(r)$  much higher than the inflow velocity  $V(r) \gg v(r)$ , therefore magnetic field does not dissipate in the parcel. Differences of turbulence evolution equations (52d), (52e), and (52f) are

$$2u\Delta u - \frac{2}{3}u^2 \frac{\Delta \rho}{\rho} = \frac{\Delta r}{vL} (c_{uu}u^3 - c_{uB11}(v_A^2 + 2v_{A\perp}^2)u \exp(-\xi)) \quad (\text{C11a})$$

$$\Delta(\rho v_A^2) + 4\rho v_A^2 \left( \frac{\Delta r}{r} - \frac{\Delta b}{b} \right) = \frac{\rho \Delta r}{vL} (c_{BB11}v_A^3 \exp(-\xi) - (c_{Bu11}v_{Ar}^2 + 2c_{Bu22}v_{Ar}v_{A\perp})u) \quad (\text{C11b})$$

$$\begin{aligned} \Delta(\rho v_{A\perp}^2) + 2\rho v_{A\perp}^2 \left( \frac{\Delta r}{r} + \frac{\Delta v}{v} - \frac{\Delta a}{a} - \frac{\Delta b}{b} \right) = \\ = \frac{\rho \Delta r}{vL} (c_{BB11}v_{A\perp}^3 \exp(-\xi) - ((c_{Bu11} + c_{Bu22})v_{A\perp}^2 - c_{Bu22}v_{Ar}v_{A\perp})u). \end{aligned} \quad (\text{C11c})$$

Magnetic helicity variation does not directly influence the dynamics of the blob. Solving the system of 7 equations (C4), (C7), (C8), (C10), (C11abc) on 7 quantities  $\Delta T, \Delta \rho, \Delta v_A, \Delta v_{A\perp}, \Delta u, \Delta a, \Delta b$ , I obtain

$$\frac{\Delta \rho_{\text{correct}}}{\rho \Delta r} \approx v_{Ar} \frac{2.02 \exp(-\xi) v_{Ar} v_{A\perp} (v_{Ar} + 2v_{A\perp}) - u(0.39(v_{Ar}^2 v_{A\perp} + v_{A\perp}^3) + v_{Ar}(1.21v_{A\perp}^2 - 0.63u^2))}{c_s^2 L v (v_{Ar}^2 + v_{A\perp}^2)}. \quad (\text{C12})$$

The actual expression is much longer. I take only the largest terms in the numerator and the denominator.

Let me compare this result (eq. [C12]) with the naive estimate, when magnetic field dissipation increases gas internal energy only (Bisnovatyi-Kogan & Ruzmaikin 1974), and gas pressure balance is used instead of parallel and perpendicular pressure balances (C4), (C7). Gas pressure balance is

$$\Delta(\rho T) = 0. \quad (\text{C13})$$

Naive heat balance (16) for the unit mass is

$$\frac{R}{\rho\mu} \left( \frac{3}{2} \rho \Delta T - T \Delta \rho \right) \approx \frac{\Delta r}{Lv} (0.41 v_{Ar}^2 u + 1.16 v_{Ar} u v_{A\perp} + 1.4 u v_{A\perp}^2 - 3.03 (v_{Ar}^3 + 2 v_{A\perp}^3) \exp(-\xi) - 1.14 u^3) \quad (\text{C14})$$

Eliminating  $\Delta T$  from relations (C13) and (C14), I find

$$\frac{1}{\rho} \frac{\Delta \rho_{\text{naive}}}{\Delta r} \approx \frac{0.61 (v_{Ar}^3 + 2 v_{A\perp}^3) \exp(-\xi) + 0.23 u^3 - 0.82 v_{Ar}^2 u - 0.23 v_{Ar} u v_{A\perp} - 0.28 u v_{A\perp}^2}{c_s^2 L v} \quad (\text{C15})$$

I evaluate the convective derivatives of density (C12) and (C15) in the inner region of the reference solution with angular momentum transport (subsection 4.2). Parameters of the reference model are  $\xi_\infty = 0.025$ ,  $\sigma_\infty = 1$ ,  $\gamma = 1$ , non-relativistic EOS. Correspondent velocities are shown on Figure 5b. I take the values (B10) of velocities and magnetic helicity on the inner boundary of integration at  $r = 3 \times 10^{-4} r_B \approx 90 r_g$ . Change of density appears to be negative  $\Delta \rho < 0$  for  $\Delta r > 0$  in the result of full calculation (eq. [C12]). Naive calculation shows positive  $\Delta \rho > 0$  for  $\Delta r > 0$ .

$$\frac{\Delta \rho_{\text{correct}}}{\Delta \rho_{\text{naive}}} \approx -0.2. \quad (\text{C16})$$

Naive calculation suggests that the flow is convectively unstable, whereas the full calculation under reasonable assumptions indicates a convectively stable flow.

The calculated result (C16) is applicable only to the inner regions of solution with angular momentum transport (subsection 4.2). Excluded external driving is important in the outer regions. In turn, solution with maximum accretion rate has large inflow velocity  $v$  that approaches gas sound speed  $c_s$ , and convection is suppressed (subsection 5.4). As a bottom line, either flow appears to be convectively stable on average or convection is suppressed in all calculated solutions without electron conductivity.

However, numerical simulations by (Igumenshchev 2006) of non-rotating flows find evidence of convection. This convection may be physical. My model averages heat from all dissipation events over the fluid. Local reconnection events can lead to burst-type local heating that leads to buoyancy of blobs. Also, magnetic buoyancy and diffusion play important role in transfer processes (Igumenshchev 2006). The correct inclusion of convection, magnetic buoyancy and diffusion is the subject of future studies.

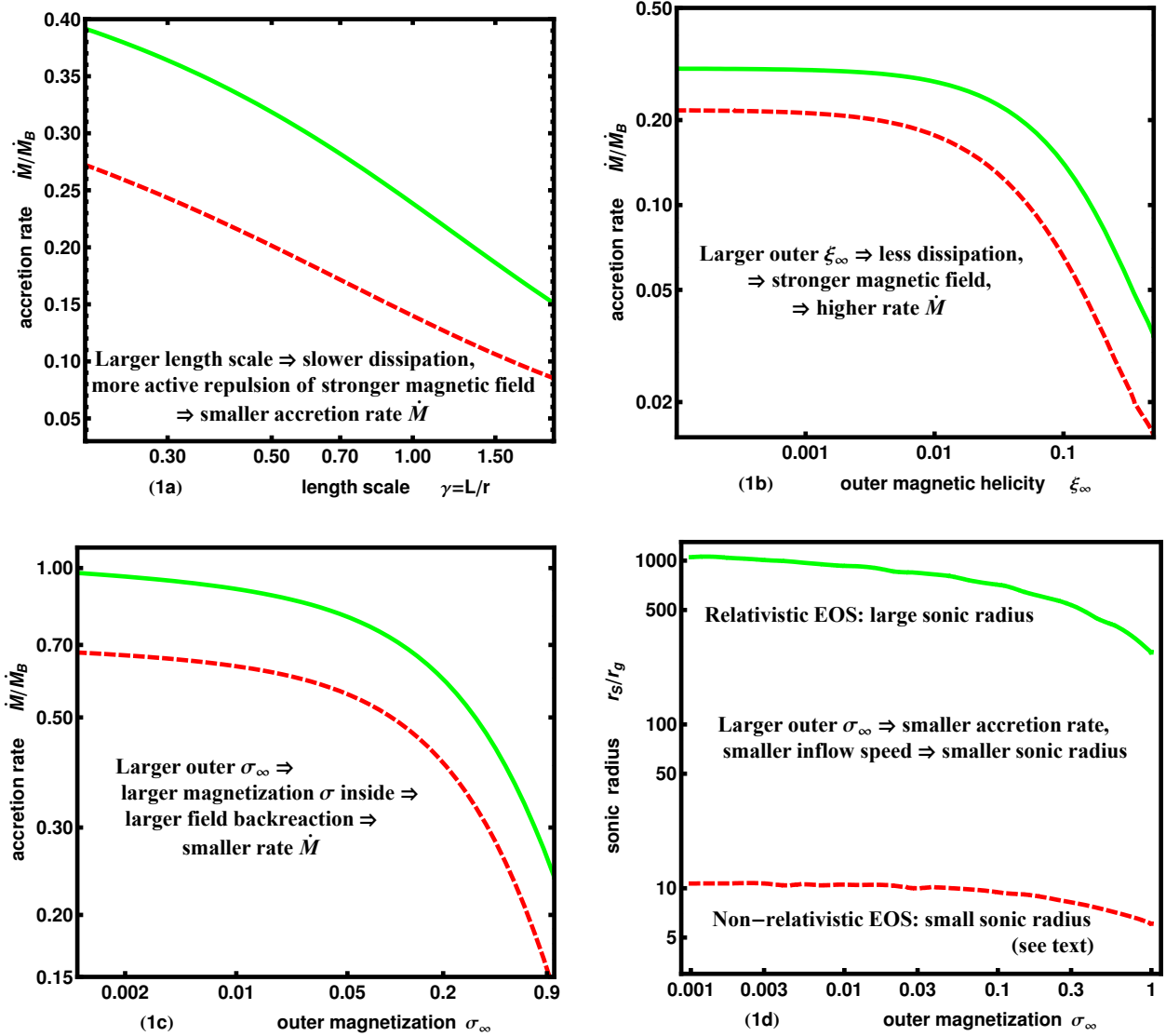


Fig. 1.— **Maximum accretion rate solution.** Dependence of the accretion rate in units of Bondi rate on dimensionless parameters: characteristic length scale  $\gamma$  (Fig. 1a), outer magnetic helicity  $\xi_\infty$  (Fig. 1b), outer matter magnetization  $\sigma_\infty$  (Fig. 1c). Dependence (Fig. 1d) of sonic radius on outer magnetization  $\sigma_\infty$ . I take the reference model to have the following values of parameters:  $\gamma = 1$ ,  $\sigma_\infty = 1$ ,  $\xi_\infty = 0.025$ . One parameter is varied to make one plot. Non-relativistic 1-T equation of state (dashed) versus relativistic 1-T equation of state (solid).

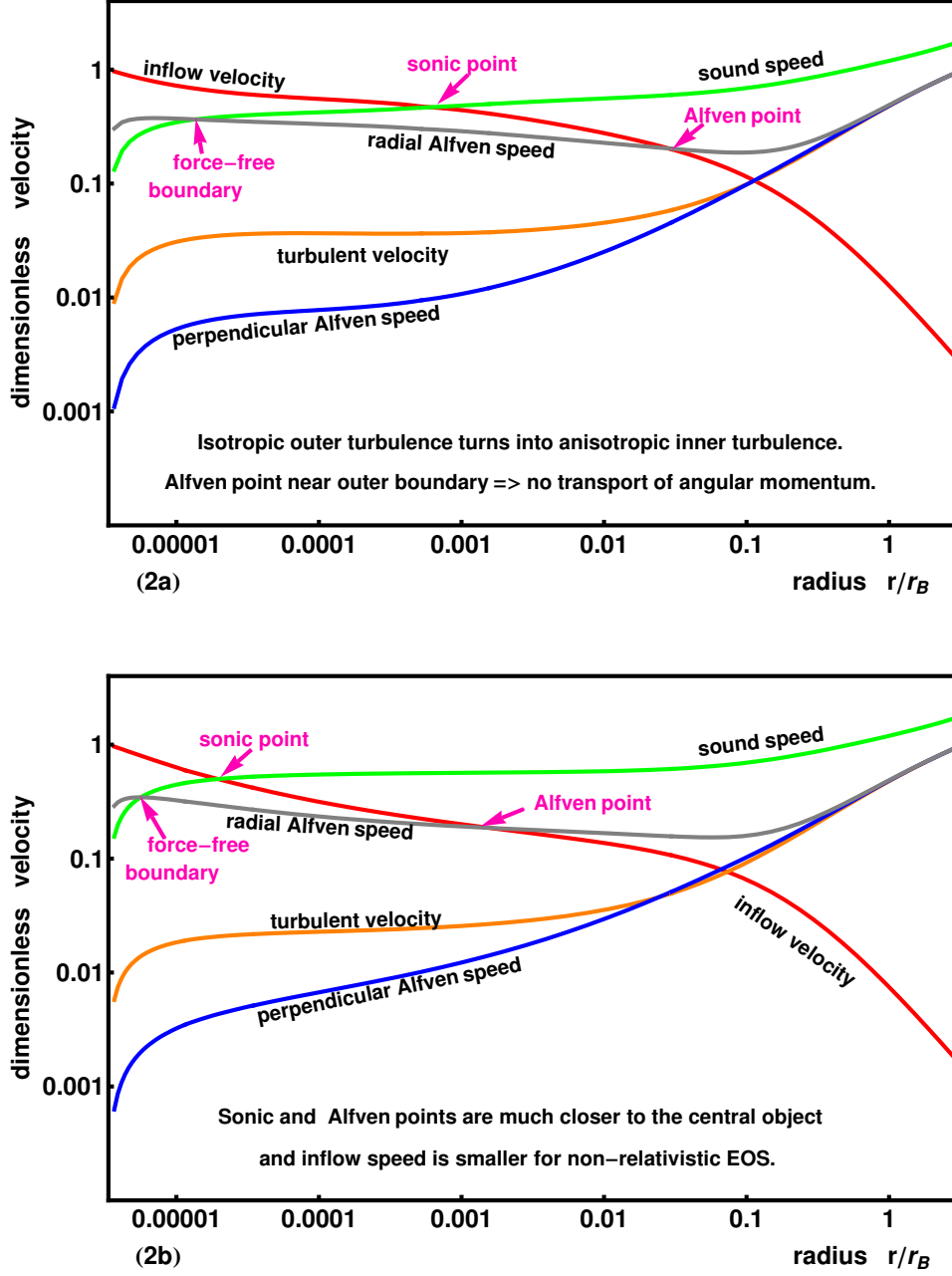


Fig. 2.— Flow velocities, normalized to free-fall speed versus radius for **maximum-rate solution**: sound speed, inflow velocity, radial Alfvén speed, 1-D perpendicular Alfvén speed, turbulent velocity. Parameters  $\sigma_\infty = 1$ ,  $\gamma = 1$ ,  $\xi_\infty = 0.025$ . Relativistic 1-T equation of state is on Figure 2a, non-relativistic 1-T EOS is on Figure 2b.

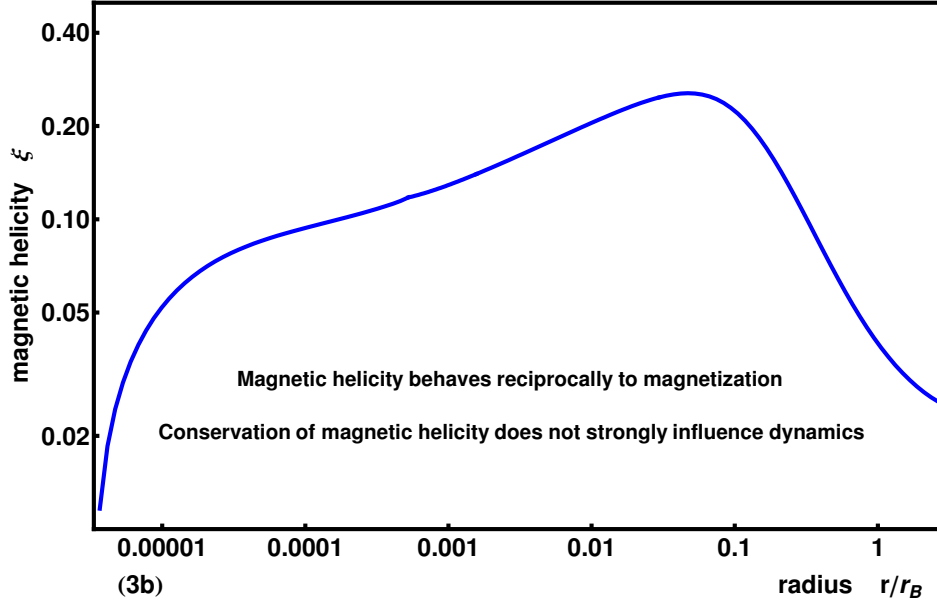
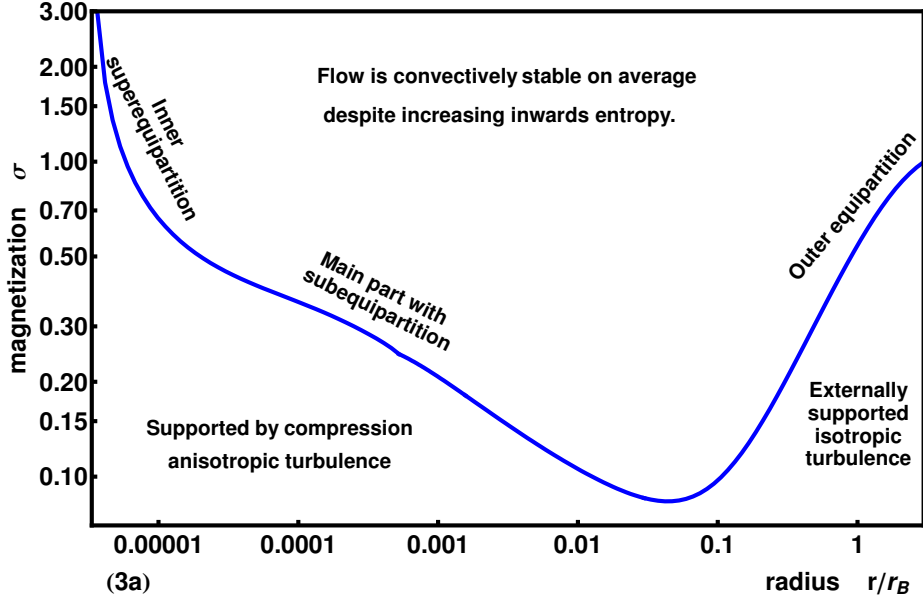


Fig. 3.— Magnetization  $\sigma$  versus dimensionless distance from the compact object  $r/r_B$  is on Figure 3a. Dimensionless magnetic helicity  $\xi$  versus dimensionless distance from the compact object  $r/r_B$  is on Figure 3b. Both are for the **maximum-rate solution** with relativistic equation of state.



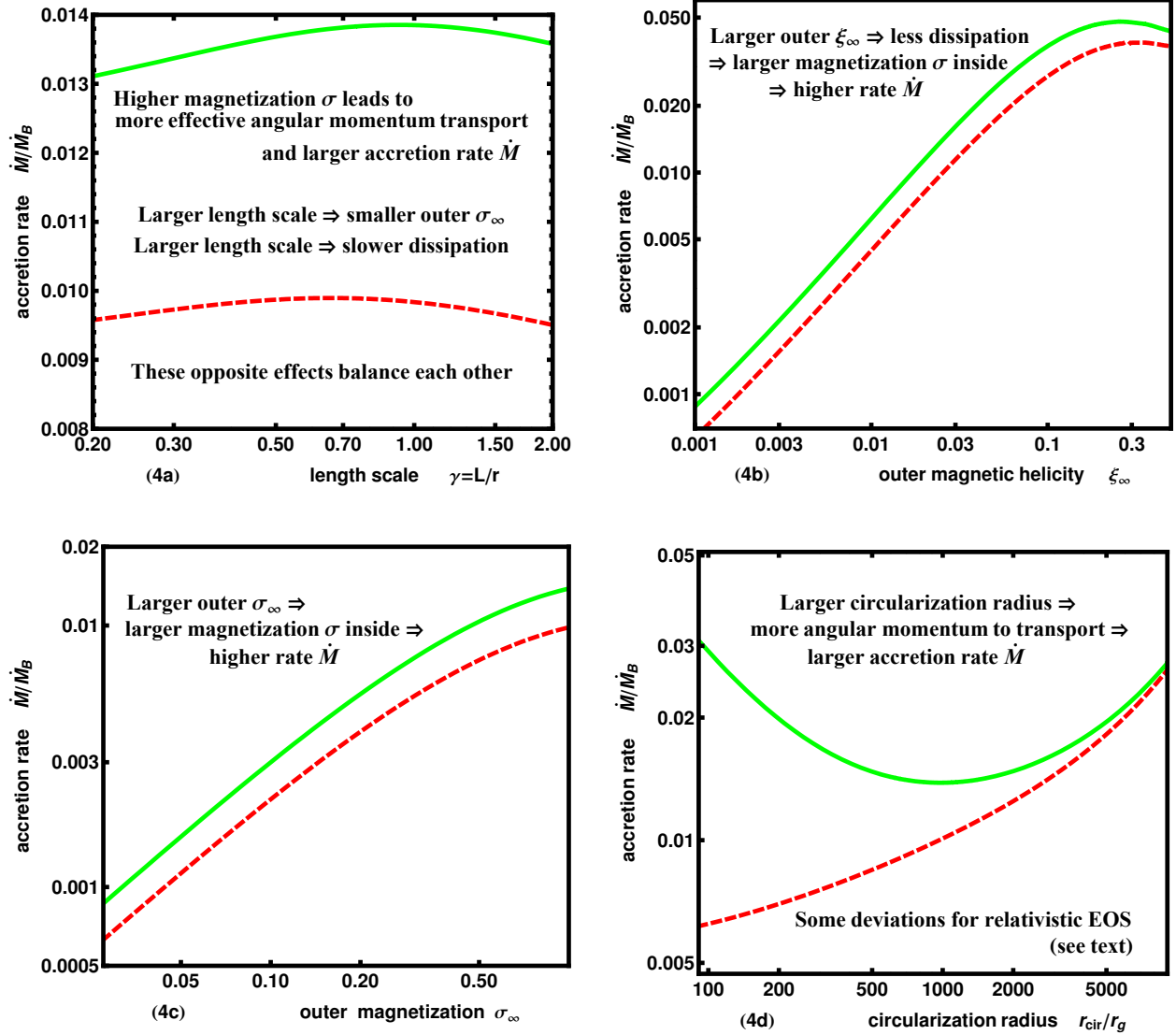


Fig. 4.— **Solution with angular momentum transport.** Dependence of the accretion rate in units of Bondi rate on dimensionless parameters: characteristic length scale  $\gamma$  (Fig. 4a), outer magnetic helicity  $\xi_\infty$  (Fig. 4b), outer magnetization  $\sigma_\infty$  (Fig. 4c), and circularization radius  $r_{\text{cir}}$  in units of  $r_g$  (Fig. 4d). I take the reference model to have the following parameters:  $\gamma = 1$ ,  $\sigma_\infty = 1$ ,  $r_{\text{cir}} = 10^3 r_g$ ,  $\xi_\infty = 0.025$ . Non-relativistic 1-T equation of state (dashed) versus relativistic 1-T equation of state (solid).

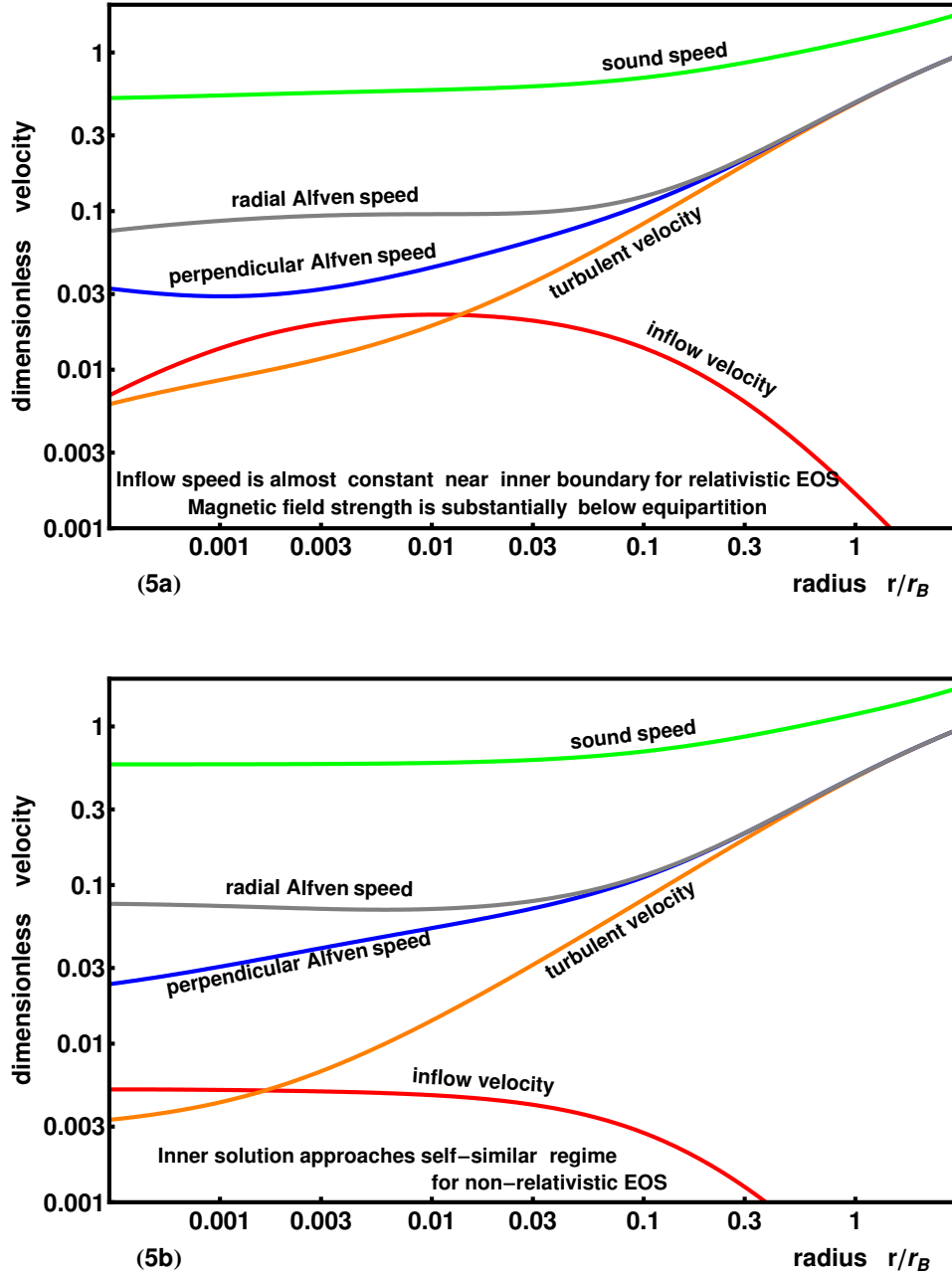


Fig. 5.— Flow velocities, normalized to free-fall speed versus radius for **solution with angular momentum transport**: sound speed, inflow velocity, radial Alfvén speed, 1-D perpendicular Alfvén speed, turbulent velocity. Parameters  $\sigma_\infty = 1$ ,  $\gamma = 1$ ,  $\xi = 0.025$ ,  $r_{\text{cir}} = 10^3 r_g$ . Relativistic 1-T EOS on Figure 5a, non-relativistic 1-T EOS on Figure 5b.

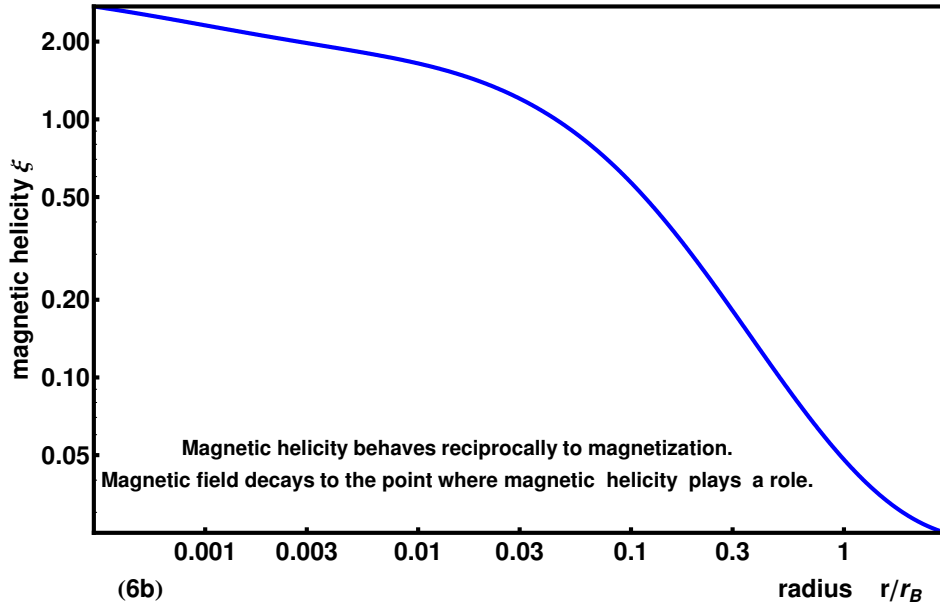
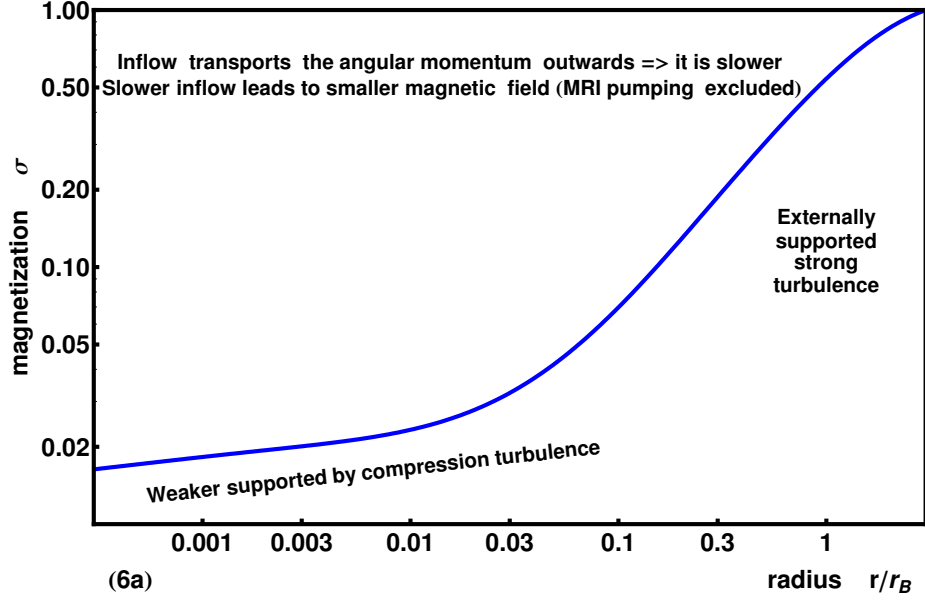


Fig. 6.— Magnetization  $\sigma$  versus dimensionless distance from the compact object  $r/r_B$  is on Figure 6a. Dimensionless magnetic helicity  $\xi$  versus dimensionless distance from the compact object  $r/r_B$  is on Figure 6b. Both are for **solution with angular momentum transport**. Circularization radius is  $r_{\text{cir}} = 10^3 r_g$ .

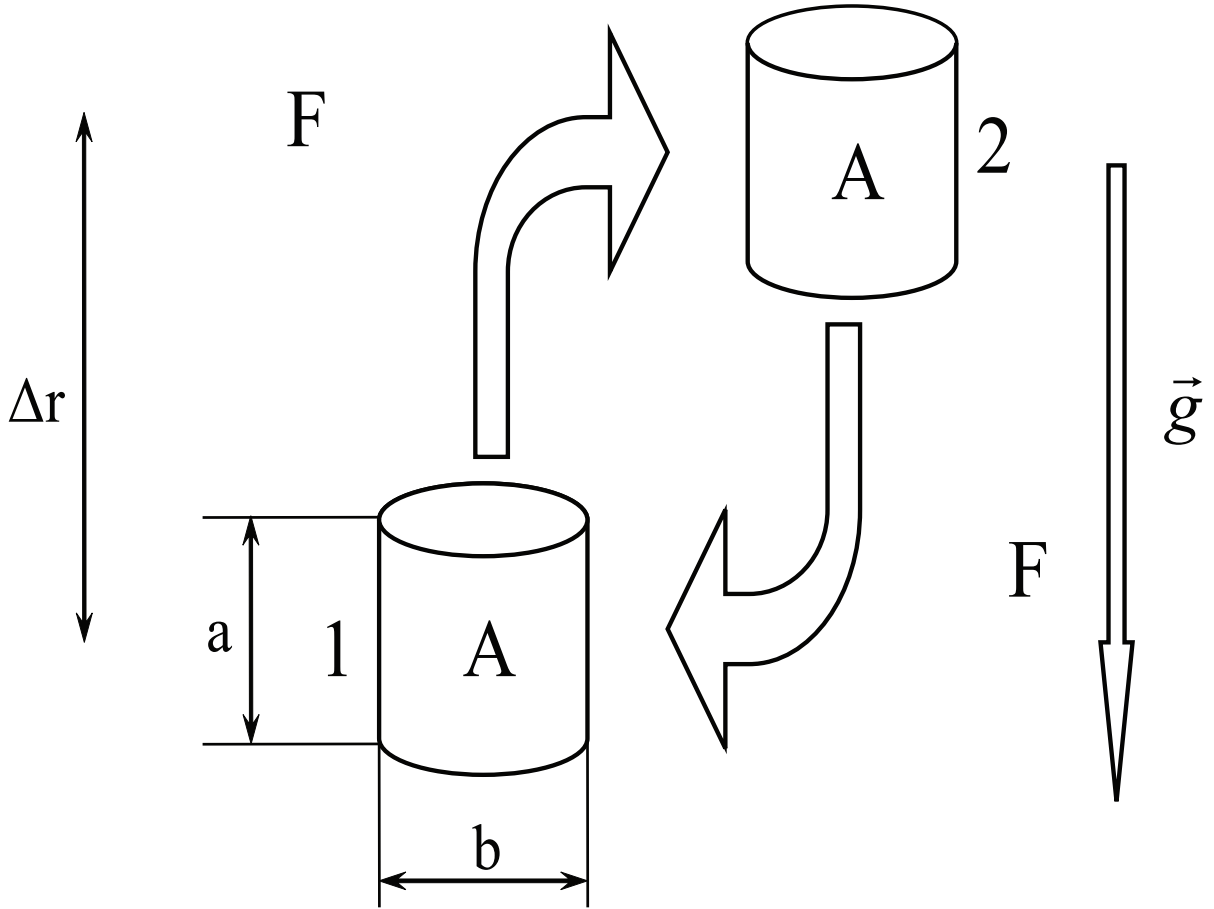


Fig. 7.— Scheme of convection. Large magnetized blob is in perpendicular and radial pressure balance. Energy does not dissipate inside the blob.